coatings

MDPI

Article

Factors Affecting the Strength Formation Mechanism and Water Stability of Geopolymer Stabilized Phosphogypsum in Road Construction

Yi Wu [1], Hanbin Zhang [1,*], Haikun Lin [2,3], Xueting Wu [1,*], Heng Li [4], Yamei Liu [1], Gonghui Gu [5], Jin Xu [1], Shengying Chen [1], Haojun Tang [1], Hualuo He [1], Wenkai Zheng [1] and Fang Xu [1,*]

[1] Faculty of Engineering, China University of Geosciences, Wuhan 430074, China; yiwu@cug.edu.cn (Y.W.); liuym199909@163.com (Y.L.); jinxu@cug.edu.cn (J.X.); csxcug9@163.com (S.C.); 17786112143@163.com (H.T.); hhl1234567892020@163.com (H.H.); wenkai574@gmail.com (W.Z.)
[2] PetroChina Coalbed Methane Company Limited, Beijing 100028, China; linhk_cbm@petrochina.com.cn
[3] China United Coalbed Methane National Engineering Research Center Co, Ltd., Beijing 100095, China
[4] College of Civil Engineering, Hunan University, Changsha 410082, China; hengli@hnu.edu.cn
[5] School of Transportation, Southeast University, Nanjing 211189, China; gugonghui@seu.edu.cn
* Correspondence: hanbinzhang898@sina.com (H.Z.); wuxueting@cug.edu.cn (X.W.); xufang@cug.edu.cn (F.X.)

Abstract: By adjusting the content of geopolymer in geopolymer stabilized phosphogypsum (GSP) as roadbed filler, along with the mixing ratio, this paper mainly explores tendencies in the mechanical properties and water stability of GSP. This research is based on macro-mechanical properties such as unconfined compressive strength, resilience modulus, California bearing ratio and shear strength. It is also based on water stability tests, such as the water soaking test, dry and wet cycle test and expansion test, to explore changes in water stability. As for the durability of GSP, this paper is mainly based on the realization of a long time observation of mechanical properties and water stability. In the existing research, most of the stabilized phosphogypsum (PG) base material or roadbed filler consists of cement, lime, etc. In this paper, a new exploration is carried out on the composition of stabilized PG material, realized without the participation of cement. The 28 d compressive strength of GSP reaches 2.5 MPa, and over time this strength grows, which prevents the phenomenon of strength inversion that may occur in conventional cement-stabilized PG. In addition, a long-term soaking experiment was designed in this study based on the material after the strength was stabilized for up to 90 d. After the strength was steady, the GSP with the best water stability still had a softening coefficient of 80% after experiencing water immersion for 7 d. After determining the feasibility of the mechanical properties and water stability of GSP as roadbed filler, we further explored the strength formation mechanism of GSP by microscopic tests (XRD and SEM). This shows that geopolymer can stabilize PG in two main ways: one is the hydration reaction with PG to generate C-S-H gel and ettringite, and the other is to connect PG not involved in the chemical reaction to form a dense whole through generated hydration products. Geopolymer, stabilizing a high amount of PG, not only provides a new method for the consumption of PG, but also has more stable performance than cement, and has certain advantages in economy. In addition, the advantage of this study is that good performance can be achieved by simply sieving PG and adjusting the geopolymer ratio in practical engineering projects.

Keywords: phosphogypsum; geopolymer; geopolymer stabilized phosphogypsum; mechanical properties; water stability; strength formation mechanism

Citation: Wu, Y.; Zhang, H.; Lin, H.; Wu, X.; Li, H.; Liu, Y.; Gu, G.; Xu, J.; Chen, S.; Tang, H.; et al. Factors Affecting the Strength Formation Mechanism and Water Stability of Geopolymer Stabilized Phosphogypsum in Road Construction. *Coatings* **2023**, *13*, 1652. https://doi.org/10.3390/coatings13091652

Academic Editor: Valeria Vignali

Received: 31 July 2023
Revised: 13 September 2023
Accepted: 15 September 2023
Published: 20 September 2023

1. Introduction

Phosphogypsum (PG) is a kind of industrial solid waste residue that is generated during the wet production of phosphoric acid. The main mineral composition of PG is $CaSO_4 \cdot 2H_2O$, and it is currently employed mostly in the field of building materials and

the chemical industry [1]. PG has a complex chemical makeup and contains impurities, including phosphorus (P), fluoride (F), and heavy metals [2–5]. The influence of impurities severely restricts the utilization of PG, leading its storage capacity to increase year after year [6]. The total amount of PG stockpiles has surpassed 500 million tons in China [7]. Due to its high inventories and low utilization rates, PG is frequently stored outdoors, which causes many issues, like environmental pollution and the waste of land resources [8–12]. Additionally, common building materials, like cement and stone, result in resource overuse and significant emissions of greenhouse gases, like CO_2. Therefore, it is particularly important to effectively promote the harmless resource utilization of PG in the field of building materials, which is of great significance in achieving the goals of energy conservation, emission reduction, and total carbon emission control.

The current comprehensive application of PG is still limited. There is an urgent need to expand new methods of using a significant amount of PG. In China, establishing roadbeds requires a significant amount of soil and stone, which are becoming increasingly expensive and rare due to over-exploitation and other issues. The problem is that the excessive use of these materials has increased economic expenses and caused a shortage of resources. Using PG as a road construction material is currently an effective way to save soil resources and consume a large amount of PG. With so many kilometers of roadways in China, there is still a significant amount of space for PG to be utilized in roadbed engineering and to increase its effective utilization rate. Due to its location beneath the surface of the road and exposure to both surface water and groundwater, the roadbed must have a certain level of strength and excellent water stability. Since PG is an air-hardening material with low strength and poor water resistance, it cannot be utilized as a roadbed filler directly. When 100% pure PG is utilized to prepare the sample of road material, although the physical compaction force given to it can aid in its shaping, it has been fractured during the demolding process [13]. Furthermore, PG has very little water resistance due to its low solubility (2.04 g/L). Moreover, PG's lower pH value and the presence of soluble phosphorus impurities make it more sensitive to water. As a result, PG cannot be used as a roadbed filler on its own. PG is suggested to be utilized only in areas away from water bodies [14].

Several researchers have increasingly used PG in the subgrade, base, or subbase fields as research into PG has become more in-depth [15,16]. PG-based cementitious materials were developed by substituting some of the cement with PG [17]. It has been demonstrated that the addition of a tiny amount of PG can boost the curing effect of soil to a certain degree [18]. Shen et al. [19] used PG in road materials, combined with steel slag and fly ash (FA) to prepare a road base material composed of all solid waste, and showed that the best curing effect was obtained when the steel slag to FA ratio was 1:1, and the content of PG was 2.5%. Only in recent years have researchers began to try to use PG as a stabilized soil material on a large scale. Ngo et al. [13] used cement and lime as curing agents to solidify PG mixed with FA, in which the content of PG was up to 90%. Additionally, the mechanical properties and environmental properties of the stabilized materials were investigated and it was proved that the stabilized PG materials met all the performance requirements. According to research by Parreira et al. [20], cement-stabilized PG mixtures have the potential for use as road base and subbase materials for paving. The study also investigates the effects of various cement types and cement content (5%, 10%, 15%) on the mechanical properties of stabilized PG materials. To avoid using cement-stabilized PG, Meskini et al. [14] prepared a type of lime FA road base material by mixing 40%–80% PG, 20%–60% FA, and 4%–20% lime. Quicklime served as the activator for the silica-aluminum FA. This stabilized road material performs best when the ratio of PG to FA is 1:1. When PG content is up to 76%, the material's mechanical properties and durability are noticeably worse than those of road material with a PG content of 40%, and the unconfined compression strength is not higher than 1.5 MPa. To stabilize a significant amount of untreated PG (87%–91%) and prepare a subbase material, Liu et al. [21] discovered that 9%

calcined PG mixed with quicklime (0%–4%) had a 28d unconfined compression strength of 1.7–4.3 MPa.

The main purpose of this study is to seek a cementitious material to replace conventional alkaline materials (such as cement, lime, etc.) to stabilize large amounts of PG and investigate the stabilizing effect of different variables of this cementitious material on PG. Mechanical properties of roadbed filler are significantly less important than those of water stability and environmental safety. To stabilize and modify PG, which has the main drawback of being used as a roadbed filler, a type of cementitious material with fast hardening and early strength, acid and alkali resistance, low permeability, corrosion resistance, good durability, and excellent heavy-metal solidification ability should be chosen.

Currently, cement has been employed as the curing agent in these studies on the utilization of PG in significant amounts as roadbed filler or road base material. As a calcium-based material, cement is easily carbonized and lacks durability. As a result, cement stabilized material has high permeability, heavy metal leaching concentration, and high-cost disadvantages, and the process of cement production generates huge amounts of CO_2, which contributes to environmental pollution [22]. FA and Granulated blast-furnace slag (GBFS) is one of the key raw materials used to make geopolymer, an alkali-activated cementitious material that was initially proposed by Davidovits et al. [23]. The two most commonly used alkali-activators for geopolymers are water glass and NaOH. Under the impact of alkali activation, part of the Si-O bonds with Al-O bonds in vitreous FA and GBFS break and condense into a three-dimensional mesh structure with a high degree of polymerization [24–26], which is an inorganic low-carbon non-metallic binding material. Not only is geopolymer more economical than ordinary Portland cement, but it also offers superior mechanical properties [27]. As a result, geopolymer is an effective way to improve PG's poor water stability and cure its heavy metals. Based on the excellent properties of geopolymers, if PG is used in the roadbed and stabilized by geopolymers, no treatment of PG is necessary other than simple sieving, which substantially minimizes the treatment processes and engineering expenses.

PG is mostly utilized for generating road base materials, according to current applications and research, and its utilization rate is not very high. Because base material is more easily contacted by water than roadbed filler, this study attempts to use a significant amount of PG in the research of roadbed filler, with the original purpose of improving the utilization rate of PG in the field of road materials. Additionally, the geopolymer, which is greener and more environmentally friendly, is used as the curing agent of this composite. The mechanical properties of PG as road material have been the subject of many studies; however, water stability and durability have received less attention. Additionally, few studies have focused on the impact of stabilizing materials on the performance of PG as a roadbed filler.

Based on the above background, silica-aluminum industrial solid waste is used as the major raw material in this study to prepare geopolymer cementitious materials. By using geopolymer to stabilize a significant amount of PG, which makes up a significant proportion of the stabilized body as soil, GSP was prepared. The mechanical properties and water stability of the GSP are two significant aspects that are investigated in this research. Following an investigation into the effects of various geopolymer ratios and PG content, the relationship between the mechanical properties and water stability is elucidated. Microscopic studies were used to further elucidate the strength formation mechanism of GSP. The GSP meets the fundamental specifications for roadbed filler in terms of mechanical properties and water stability. Furthermore, this study reveals how GSP develops its strength and maintains its water stability. A large amount of PG is consumed, providing a new method for resource utilization of PG, which actively responds to the national policy call to explore the application of PG in the field of roadbed materials, with significant economic and social benefits.

2. Experimental Test

2.1. Materials

The two components of the raw materials used in this study are as follows: geopolymer as curing agent and PG as stabilized fine aggregate. The geopolymer was made by utilizing two industrial solid waste raw materials, FA and GBFS, both of which contain silica-aluminum as the major component. The alkali-activator was made by mixing NaOH dissolved in water glass. PG was produced as a fine soil sieved after a 4.75 mm standard sieve. Table 1 shows the chemical composition of FA, GBFS, and PG samples measured by X-ray fluorescence spectroscopy (XRF).

Table 1. Chemical composition of raw materials (wt.%).

Material	SiO_2	Al_2O_3	CaO	SO_3	Fe_2O_3	MnO	MgO	Na_2O	K_2O	P_2O_5	TiO_2	Loss
FA	35.01	21.09	27.56	/	0.32	0.16	12.87	0.36	0.27	0.05	0.26	1.49
GBFS	50.45	38.64	2.93	/	3.22	0.04	1.9	1.52	0.54	0.2	0.38	3.49
PG	16.31	3.68	25.89	40.91	0.73	0	0.93	2.45	0.77	0.87	0.07	22.95

The experiments were conducted using grade II PG from Hubei Zhongfu Chemical Group Co., Ltd. in Yichang, China. that met the requirements of phosphogypsum (GB/T 23456-2018) [28] and was in the form of grey granules with a particle distribution of fine powder below 4.75 mm. The main chemical components of PG are CaO, SO_3, and SiO_2. Figure 1a demonstrates that the major mineral composition of PG is $CaSO_4 \cdot 2H_2O$. The microstructure morphology of PG (in Figure 1b) shows that the $CaSO_4 \cdot 2H_2O$ crystalline structure consists of regular short columns with impurity components on the surface or overlay.

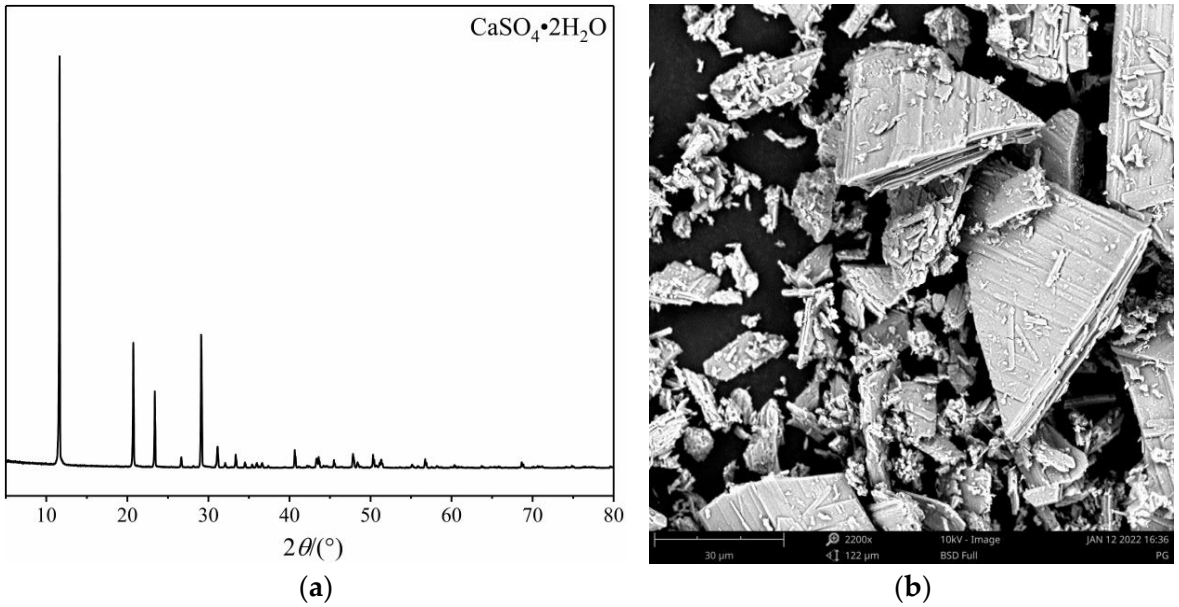

(**a**) (**b**)

Figure 1. XRD (**a**) and SEM (**b**) of PG.

The S95 GBFS was produced by Wuhan Iron and Steel Co., Ltd in Wuhan, China. with a 0.045 mm square hole sieve residue of 2.3% and a specific surface area of 426 m^2/kg. CaO, Al_2O_3, and SiO_2 make up most of the chemical composition of GBFS. The main mineral component of GBFS is an amorphous material with a glassy texture.

The FA has a fineness of 0.045 mm, a square hole sieve residue of 10.7%, and is a national grade I low calcium FA made in Zhongshan, Guangdong Province. CaO, Al_2O_3, SiO_2, and MgO are its primary chemical constituents.

Mixing NaOH dissolved in a water glass prepared the alkali-activator used in the experiments [29–33]. The prepared geopolymer cementitious material performed better after the modulus was changed to 1.2 by adding 20.3 g NaOH per 100 g of water glass. The analytical purity of the NaOH, which was provided by Tianjin Beilian (Tianjin, China), was higher than 96%. Table 2 lists the specific parameters of the water glass.

Table 2. The parameters of water glass.

Colour	Modulus	Pomerol	Na_2O (%)	SiO_2 (%)
Colorless transparent liquid	3.24	39.5	9.25	29

2.2. Mix Proportions

According to research by Xu et al. [31], the mechanical and overall properties of the prepared geopolymer were better when the solid alkali-activator content was between 11%–14%, and the long-term strength of the geopolymer was developed best at 11%. Based on this, we first explored the mechanical properties of geopolymers as curing agents, and selected four geopolymer ratios with excellent mechanical properties as curing agents for large amounts of PG. The preparation of geopolymer slurry is shown in Figure 2, and its mix design and compressive strength are shown in Table 3.

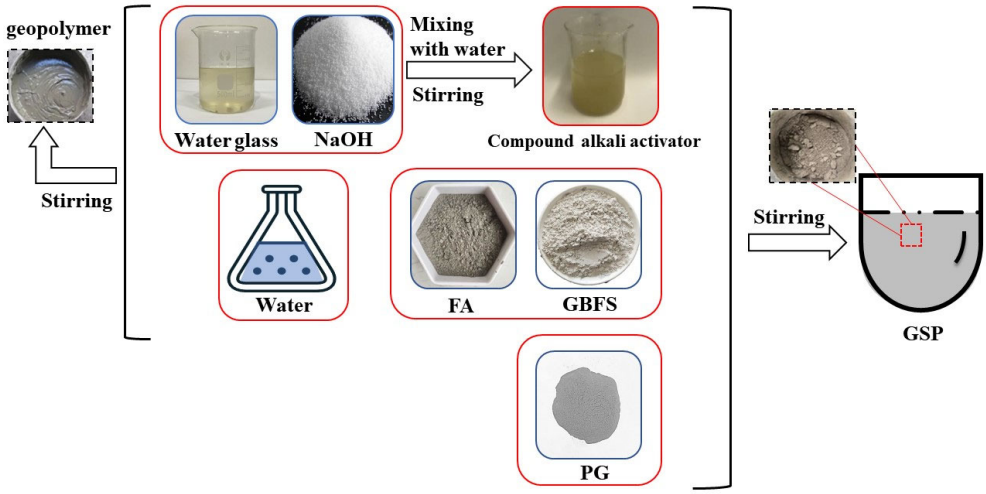

Figure 2. Preparation of geopolymer and GSP.

Table 3. Mix ratio and 28 d compressive strength of geopolymer.

Sample	FA (%)	GBFS (%)	Solid Activator (%)	Water-to-Solid	28 d Compressive Strength
M	25	75	11%	0.3	50.84
N	30	70	11%	0.3	55.71
K	35	65	11%	0.3	45.11
C	40	60	11%	0.3	70.93
F	45	55	11%	0.3	49.97
E	50	50	11%	0.3	46.01
S	55	45	11%	0.3	61.67
H	60	40	11%	0.3	54.83
J	60	40	14%	0.3	77.99

Through exploring the mechanical properties of geopolymers, we have designed the ratio of GSP. The amounts of PG used in the mix design in Table 4 are intended to be 90%, 94%, and 98%, respectively. For the alkali-activator in the geopolymer, NaOH is used to modify the sodium silicate's modulus to 1.2, the amount of solid alkali-activator is 11%

and 14%, and the mass percentage of FA in the curing agent is steadily rising (30%, 40%, and 55%).

Table 4. Mix ratio of GSP.

Sample	Geopolymer (wt%)	PG (wt%)	Composition in Geopolymer		
			FA (wt%)	GBFS (wt%)	Alkali-Activator (wt%)
P90-G(30:70)-C11	10	90			
P94-G(30:70)-C11	6	94	30	70	11
P98-G(30:70)-C11	2	98			
P90-G(40:60)-C11	10	90			
P94-G(40:60)-C11	6	94	40	60	11
P98-G(40:60)-C11	2	98			
P90-G(55:45)-C11	10	90			
P94-G(55:45)-C11	6	94	55	45	11
P98-G(55:45)-C11	2	98			
P90-G(55:45)-C14	10	90			
P94-G(55:45)-C14	6	94	55	45	14
P98-G(55:45)-C14	2	98			

In Tables 3 and 4, the content of the solid alkali-activator is calculated using Equation (1).

$$\text{Content of solid alkali activator} = \frac{m_{\text{alkali}}}{m_{\text{FA}} + m_{\text{GBFS}} + m_{\text{alkali}}} \quad (1)$$

In Equation (1):

m_{alkali} is the solid alkali-activator content in g;
m_{FA} is the FA content in g;
m_{GBFS} is the GBFS content in g.

Figure 2 illustrates the preparation of the GSP:

(1) Preparation of the alkali-activator: before preparing GSP, the alkali-activator should be prepared. To begin, weigh the water glass, then weigh the NaOH at a ratio of 20.3 g of NaOH for every 100 g of water glass. The NaOH should then be weighed after being dissolved in the water glass. The glass rod should next be used to stir until all of the NaOH particles have been dissolved, and then the mixture should be cooled. Water vapor will evaporate as the temperature decreases. Thus, the evaporated water ought to be added following the mixture's complete cooling.

(2) Preparation of GSP: Before sampling, the maximum dry density and optimum water content of the GSP were determined by a compaction test by the Test Methods of Soils for Highway Engineering (JTG 3430-2020) [34]. It was discovered that the optimum water content for GSP was about 20%, while the maximum dry density was around 1.5 g/cm^3. To generate GSP samples by the mix ratios in Table 3, take into account the maximum dry density and optimum water content mentioned above. Then, combine the FA, GBFS, PG, and alkali-activator in the mixer in the ratio. A cylindrical sample is generated and placed in a standard curing box for curing by the Test Methods of Materials Stabilized with Inorganic Binders for Highway Engineering (JTG E51-2009) [35]. The sample has an inner diameter of 50 mm and a height of 50 mm.

2.3. Test Methods

2.3.1. Unconfined Compressive Strength (UCS)

According to JTG E51-2009, after standard curing of the sample to the different age, place the test piece on a pavement material strength tester for the UCS test. During the test,

the loading rate should be kept at 1 mm/min. Record the maximum pressure P (N) at the time of sample failure, and calculate the UCS according with the following equation:

$$R_e = \frac{P}{A} \quad (2)$$

In Equation (2):

R_e is the UCS, in MPa;
P is the maximum pressure at the time of sample failure, in N;
A is the cross-sectional area of the sample, in mm^2.

2.3.2. Expansion and California Bearing Ratio (CBR)

Sample preparation: Place the test cylinder on a hard ground, and pour the prepared sample into the cylinder in three stages. Level the surface and slightly compress it, then compact the first layer of the sample 27 times per layer. The hammer should fall freely and vertically during compaction, and the hammer marks must be evenly distributed on the surface of the sample. After the first layer is compacted, the surface of the sample is "roughening", and then the sleeve is inserted. Repeat the above method for the compaction of each layer of sample.

Expansion: After the sample is made, a piece of filter paper is placed and a porous plate with an adjustment rod is installed on it. Four load blocks are added to the porous plate. Place the test cylinder in the slot of the porous plate instrument, and tighten the mold with a pull rod. Install a dial gauge and take the initial reading. Pour water into the sink to allow it to freely enter the top and bottom of the sample. During the soaking period, the water surface in the tank should be maintained approximately 25 mm above the top surface of the sample. Usually, the sample needs to be soaked in water for 4 d. At the end of soaking, take the final reading of the dial gauge on the sample and calculate the expansion using the following equation:

$$\text{Expansion} = \frac{\text{Changes in the height after soaking}}{\text{Initial height of the sample}} \times 100\% \quad (3)$$

Penetration test: place the sample after soaking on the lifting platform of the pavement material strength tester, so that the penetration rod fully contacts the top surface of the sample, and place four load plates around the penetration rod. Apply a 45 N load to the penetration rod first, then adjust the dial indicators for measuring force and deformation to an integer, and record the initial reading. Apply a load to press the penetration rod into the sample at a speed of 1 mm/min, and use the ratio of unit pressure to standard pressure at a penetration rate of 2.5 mm as the CBR of the material. Simultaneously calculate the CBR when the penetration is 5 mm. If the CBR at a penetration rate of 5 mm is greater than the CBR at a penetration rate of 2.5 mm, the test should be repeated. If the result remains the same, the bearing ratio at 5 mm should be used.

2.3.3. Resilient Modulus

According to JTG 3430-2020, the sample is formed using the method of Section 2.3.2. Place the sample and test cylinder on the lifting table of the strength tester, and load them to 50, 100, 150, and 200 kPa, step-by-step. Record the rebound deformation generated by the sample when loaded to each pressure. Plot and fit the obtained experimental data using pressure as the horizontal axis and rebound deformation as the vertical axis, and the slope of the fitting curve is the value of resilient modulus.

2.3.4. Cohesion Force and Internal Friction Angle

The shear strength test was conducted according to JTG 3430-2020, and six samples were prepared for each ratio using a ring cutter with an inner diameter of 61.8 mm and a height of 20 mm. Perform step-by-step loading experiments on each sample, and record

the reading of the force gauge dial gauge, until the sample is sheared. Using shear strength τ_f as the ordinate and normal stress σ as the abscissa, draw a τ_f-σ relationship curve, fit to obtain the internal friction angle φ and cohesion c, and calculate the shear strength according to the Coulomb formula: $\tau_f = \sigma tan\varphi + c$.

2.3.5. Softening Coefficient

The experimental samples are put in a standard curing box, where the UCS is measured at each age until it remains stable, recorded as R_1; after that, the stable experimental samples are soaked in water, where the UCS at each age of the soaked samples is measured, recording as R_2. Equation (4) can be used to calculate the softening coefficient (K) of samples of GSP.

$$K = \frac{R_2}{R_1} \tag{4}$$

2.3.6. Mass Loss Rate after Soaking and Average Water Absorption

Place the samples in water when it has been stabilized to a steady strength (60 d). Before soaking in water, weigh each sample and record its mass as m_0. After soaking it in water, weigh it every three days and record the result as m_1 until the mass remained stable. Then, The average water absorption after soaking is $m_1 - m_0$; using Equation (5), the Mass loss rate (MLR_s) can be calculated.

$$MLR_s = \frac{m_0 - m_1}{m_0} \times 100\% \tag{5}$$

2.3.7. Dry and Wet Cycle (DWC)

The samples will be maintained outdoors in alternating cycles with the standard curing box. The mass loss and strength loss will be tested for 5, 10, 15, 20, 25, and 30 cycles respectively, and the mass loss rate under DWC conditions will be calculated in the same way as Equation (3). Equation (6) describes how to calculate the strength loss rate under DWC conditions.

$$SLR_{DWC} = \frac{R_1 - R_{DWC}}{R_1} \times 100\% \tag{6}$$

In Equation (6):

SLR_{DWC} is the strength loss rate in % under DWC conditions;
R_1 is the UCS under standard curing conditions, in MPa;
R_{DWC} is the UCS under DWC conditions, in MPa.

2.3.8. X-ray Diffraction (XRD) and Scanning Electron Microscopy (SEM)

XRD: At a certain age, a representative small sample is taken and soaked in alcohol to terminate hydration. During testing, the sample is dried, ground into a powder with a fineness of no less than 200 mesh, and sealed in a plastic bag. The measurements were conducted using a portable X-ray diffractometer (Lailei Technology Development Co., Ltd., Shenzhen, China), model XRD-Terra. The instrument parameters are: 30 KV tube voltage, 300 μA tube current, copper target, 0.02 step width, 6000 Hz vibration frequency, 2θ range is 5°–55°.

SEM: After conducting compressive strength testing at the designated age, take crushed small pieces to make a 1 cm sized sample and grind its surface flat. After sample preparation, immerse the sample in alcohol to terminate hydration, and dry the sample before scanning electron microscopy analysis. At the beginning of the experiment, a thin layer of platinum is applied to the surface of the sample. A Phenom Pro benchtop field emission electron microscope (Funa Scientific Instruments Co., Ltd., Shanghai, China) was used to observe the microscopic morphology of GSP. The energy of the accelerator beam is 10 kv.

3. Results and Discussion

3.1. Mechanical Properties of GSP

3.1.1. California Bearing Ratio (CBR) and Resilient Modulus

Since there is a prediction model between CBR and resilient modulus, it is clear from Figure 3 that the trend for both variables is consistent. CBR can be used to predict the bigness or smallness of the resilient modulus [36]. In this study, with the same geopolymer amount, the CBR and resilience modulus of GSP declined as the FA content in the geopolymer increased. The GSP performed the best when the FA to GBFS ratio is 30:70 in geopolymer. The highest CBR and resilient modulus are found in the P94-G(30:70)-C11, reaching 7.07% and 173.06 MPa, respectively. These values are 3.47 times the CBR and 3.6 times the resilient modulus of the P94-G(55:45)-C11, respectively. At this time, the capacity to resist vertical deformation during the elastic deformation stage is stronger and can support higher loads when the material has solidified. When the amount of alkali-activator is raised from 11% to 14%, the CBR and resilient modulus of GSP are also somewhat increased. The addition of 3% alkali-activator raises the CBR by 90% and the resilient modulus by 127% when the content of PG is 94%. In addition, Figure 3 demonstrates that the CBR and resilient modulus do not diminish as the curing agent content in the GSP sample decreases. Due to the poor mechanical properties of PG, the capacity of ordinary soil foundation to resist load or deformation gets poorer as PG content increases [13]. However, we can see that the impact of various geopolymer proportions on the CBR steadily diminishes when the PG content approaches 98%. The maximum resilient modulus is 1.14 times greater than the minimum resilient modulus, and the highest CBR is 1.19 times greater than the minimum CBR in the four groups. This is sufficient evidence to demonstrate that, as PG content reaches 98%, the influence of the geopolymer on GSP is no longer immediately obvious due to the geopolymer's low content. In conclusion, the CBR of GSP samples in the other groups, except P90-G(55:45)-C11 and P90-G(40:60)-C11, is between 2% and 8%, which satisfies the minimum CBR standard value of roadbed filler in JTG/T 3610-2019 [37].

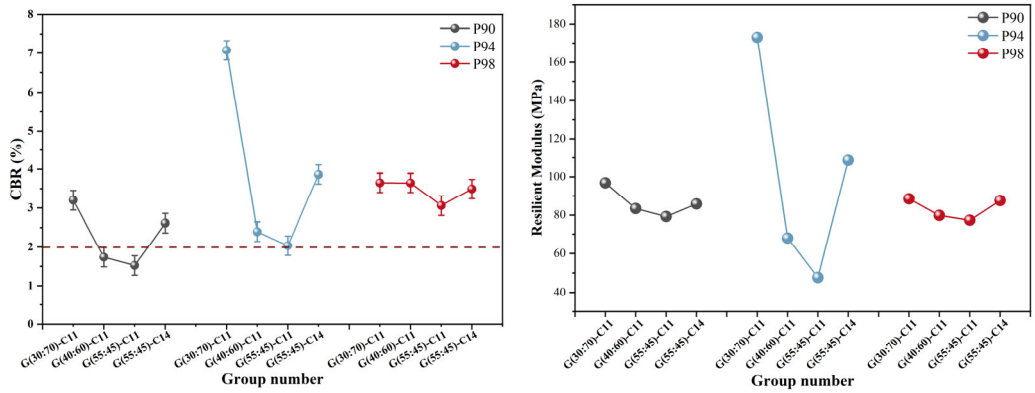

Figure 3. CBR (**a**) and resilient modulus (**b**) of GSP.

3.1.2. Unconfined Compressive Strength (UCS)

Figure 4 demonstrates how the amount of geopolymer, the curing period, and the mixing ratio of geopolymer all affect the UCS of GSP [38]. Each GSP sample's UCS gradually rises with curing age until it stabilizes at a certain value. Also, from 7 to 60 d, the UCS of GSP samples increases quickly. After 60 d, the UCS achieves a steady value and subsequently increases gradually. It is obvious why this is the case: in the late stages of the hydration process, the reactive ions in the GSP are unable to support the continuous hydration reaction because they have already been entirely consumed in the early stages of the hydration process. Moreover, Figure 4 shows that, as the amount of geopolymer is decreased, the UCS of GSP samples will likewise decline. The optimum mechanical

properties of GSP are seen when FA:GBFS = 30:70 is used as the geopolymer ratio. The P90-G(30:70)-C11 has the highest UCS, with 28d UCS developing to 2.5 MPa, which is 4.1 times that of P90-G(55:45)-C11, and 120d UCS being 3.7 MPa, which is 3.9 times that of P90-G(55:45)-C11. At the same time, we can see that a moderate rise in the alkali-activator content promotes the growth of the GSP's UCS, and that the strength will increase proportionately to the amount of geopolymer present. P90-G(55:45)-C14 has an UCS that is 1.9 times higher than P90-G(55:45)-C11, and P98-G(55:45)-C14 has an UCS that is 1.3 times higher than P98-G(55:45)-C11.

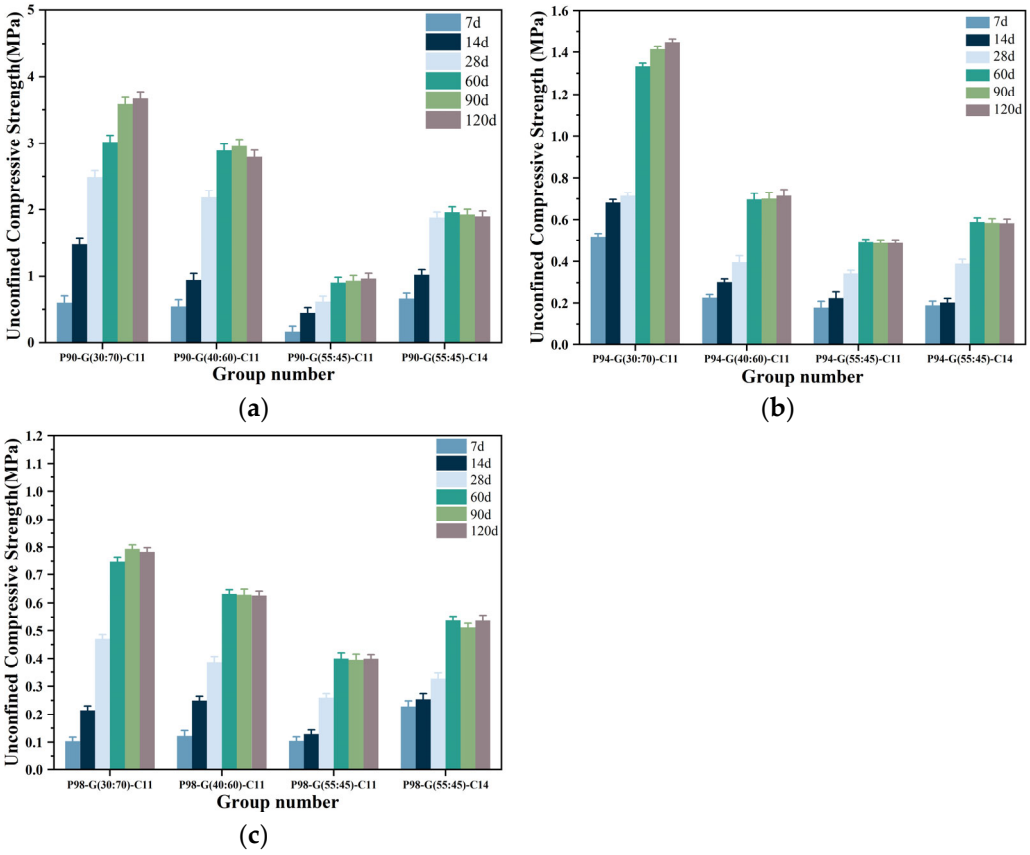

Figure 4. UCS of GSP. (**a**) GSP with 90wt% PG; (**b**) GSP with 94wt% PG; (**c**) GSP with 98wt% PG.

3.1.3. Cohesive Force and Internal Friction Angle

Figure 5 shows that, for GSP with the same PG content, the cohesive force and internal friction angle decrease as the amount of FA in the geopolymer increases. When FA:GBFS = 30:70, the cohesive force and internal friction angle of GSP achieve their highest values. The cohesive force reaches its maximum value of 102.8 kPa when the content of PG is 90%, and the internal friction angle reaches its maximum value of 30° when the content of PG is 94%. The G(55:45)-C11 group has an internal friction angle above 18° and a cohesive force below 50 kPa; it currently belongs to a weak structural plane. In contrast, all other groups of GSP, with the exception of G(55:45)-C11 group, have cohesive force values of at least 70 kPa and internal friction angles of at least 18°, all of which belong to rigid structural planes. Particularly, the cohesive force and internal friction angle of P94-G(30:70)-C11 can approach 90 kPa and 30°, respectively, showing that their structural surfaces have a good level of adhesion. When FA: GSP = 30:70 is used, the GSP exhibits greater performance of shear strength, meaning that when it is exposed to external shear pressures, its capacity to resist damage and deformation is strongest. In addition, it can be seen from the figure that adding more alkali-activator also improves the shear resistance of GSP, increasing the cohesive force by nearly two times, which makes the stabilized GSP change from a weak structural plane to a hard structural plane.

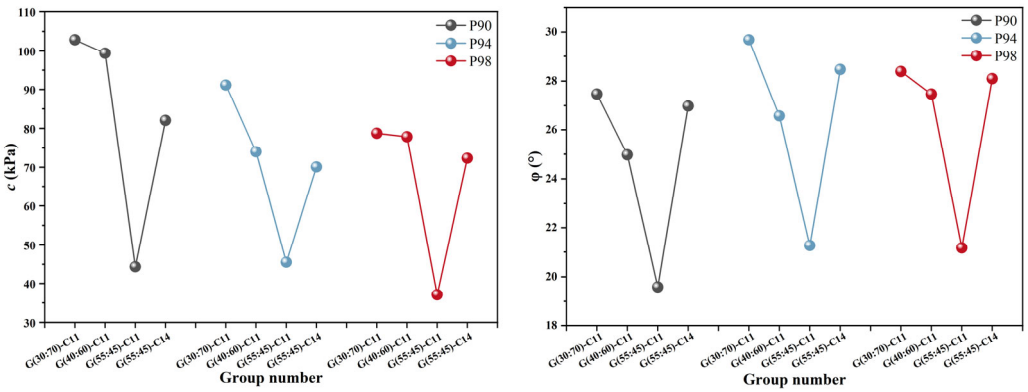

Figure 5. Cohesive force (**a**) and internal friction angle (**b**) of GSP.

3.1.4. Discussion

The changes in mechanical properties in this study shows that the overall mechanical properties of GSP mainly influenced by three aspects: (1) the ratio of FA to GBFS in the geopolymer; (2) the amount of alkali-activator in geopolymer; (3) mass percentage of geopolymer in GSP.

How does the ratio of FA to GBFS in geopolymers affects the mechanical properties of GSP? We will explain in the following. The low-calcium FA that was utilized in this study, which cannot supply a high calcium source and has no activity by itself at room temperature, leads to a slower development of early strength [39]. Low-calcium FA in the GSP primarily experienced pozzolanic reactions through alkali-activation of the water glass and sodium hydroxide; it can also produce sodium aluminosilicate (N-A-S-H) polymers, which give GSP its strength [40]. The structure of the polymer is extremely stable, but it cannot agglomerate dispersed PG particles together [41]. In addition, unlike C-(A)-S-H, N-A-S-H cannot engage in further hydration reactions with sulfate in PG to produce hydration products that support the mechanical properties of GSP. In the Ca-Na-Si-Al quaternary system, this means that, when FA content rises, the percentage of Ca^{2+} falls, while the proportion of Na^{+} rises, increasing the production of N-A-S-H polymers while decreasing the precipitations of C-S-H, C-A-H, and C-A-S-H. We believe that N-A-S-H can only serve as a stable polymer to fill the pores of GSP, and C-(A)-S-H can not only fill the pores but also bond the dispersed PG particles together. Furthermore, C-A-H can also undergo hydration reaction with PG. Based on this, as the ratio of FA to GBFS in the geopolymer increases, the mechanical properties of GSP will decrease.

The alkali-activator also affects the mechanical properties of GSP. The overall mechanical properties of GSP are improved when the amount of alkali-activator is properly increased in a certain range. The primary function of the alkali-activator in GSP is to control the pH of the hydration environment. The pH of the GSP hydration environment will affects the solubility of PG and the rate of the hydration process [9]. For one thing, the disadvantage of PG's low solubility is much more obvious at low pH. The mechanical properties and water stability of GSP are significantly impacted by PG's low solubility. The lower the pH value, the lower the solubility of PG, and the more PG dissolves. As PG dissolves, soluble phosphorus, fluorine, and heavy metal ions in PG will overflow. At the same time, it will further reduce the pH value of the hydration environment of GSP. Therefore, the solubility of PG can be improved by increasing the amount of alkali-activator, which can further improve the pH value of the hydration environment of GSP [9]. In addition, the alkali-activator also provides a small amount of silicon source, and the improvement of silicon source is conducive to promoting the formation of C-S-H, C-A-S-H, and N-A-S-H in GSP [42]. Furthermore, it can promote the precipitation of ettringite. The formation of these hydration products is beneficial for the mechanical properties of GSP.

In addition, it is necessary to dissolve the silicon-aluminum components of FA and GBFS in an environment with a sufficiently high alkalinity [43,44]. Alkali-activation, which can break and restructure the Si-O and Al-O bonds in GBFS and FA to generate a composite with cementitious properties, is actually the action of alkaline ions within the system [43]. As a result, the amount of compound alkali-activator can have a significant impact on the mechanical properties of GSP. Alkali-activator should not, however, be used in excess. First of all, too much OH^- will break the charge balance of the system, lowering the overall strength of GSP [45,46]. Secondly, under high alkalinity, hydration reactions will continue to occur, generating excessive silicate hydration products, mainly composed of ettringite. The silicate hydration products will gradually cover the PG, unreacted FA, and GBFS, preventing the following hydration reaction.

The test results for mechanical properties also show that the macroscopic mechanical properties of GSP decline as the amount of geopolymer decreases. Firstly, a decrease in the amount of geopolymer in GSP means an increase in the amount of PG. As is well known, PG itself is a material without mechanical properties. Therefore, it requires other materials to stabilize. From a physical perspective, as the PG content increases (decrease in geopolymer amount), the less that PG undergoes hydration reaction with the geopolymer, and the more unreacted PG. The decrease of hydration products with cementitious properties and the increase of dispersed PG raw materials will lead to higher porosity of GSP. From a chemical standpoint, excessive PG will lower the geopolymer's ability to polymerize and the pH of the overall hydration environment of GSP, both of which are harmful to the formation of hydration products of the GSP and ultimately lead to a decline in the GSP's overall mechanical properties [47].

3.2. Water Stability of GSP

3.2.1. Expansion and Average Water Absorption

The hydrophilic property of PG is well known [14]. The sample of GSP has a certain number and size of pores. After soaking, water can enter the interior of the GSP sample through the pores. This will cause GSP to gradually lose its mechanical properties as well as cause deformation and cracking. The sample of GSP will eventually collapse when its mechanical properties decrease to a specific point until they becomes loose from loss of resistance in the water. The higher the water absorption during the soaking process of GSP, the larger the expansion. Figure 6 shows that the expansion and average water absorption of Group G(30:70)-C11 are the lowest, whereas they are the opposite for those in Group G(55:45)-C11, showing that Group G(30:70)-C11 has the best anti-expansion performance and the strongest resistance to water erosion. The P94-G(30:70)-C11, which possesses the best mechanical qualities, also exhibits the lowest expansion and average water absorption, with values of only 1.39% and 12.4%, respectively. This shows that the stronger the ability to resist deformation after soaking, the better the bonding and structural compactness of the interface in GSP. As can be seen, with the same amount of PG, the expansion and average water absorption increase as the mass percentage of FA in the geopolymer gradually rises. The G(30:70)-C11 group with stronger mechanical properties has the strongest resistance to water erosion and may retain a certain volume stability in water. At the same time, we can observe that the expansion and water absorption of GSP increase with the higher content of PG. The average water absorption and expansion of GSP is higher when the PG content is up to 98% than when it is 90% or 94%. For example, the expansion of P98-G(30:70)-C11 is 4.6 times that of P94-G(30:70)-C11, and the water absorption increases by about 13%. Figure 6 shows that adding more alkali-activatorF to GSP enhances not only its mechanical properties but also its volume stability in water. The expansion of the P98-G(55:45)-C14 decreased by almost 54% when compared to the P98-G(55:45)-C11, and the water absorption is decreased by 11% with a 3% increase in alkali-activator.

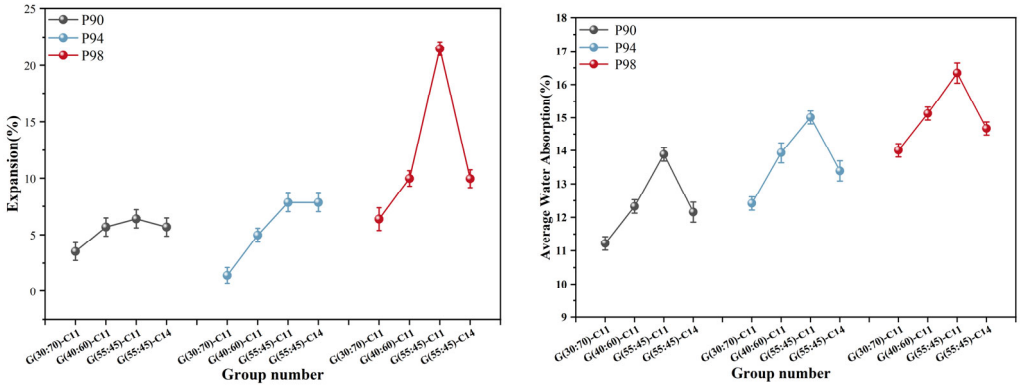

Figure 6. Expansion (**a**) and average water absorption (**b**) of GSP.

A higher water absorption and expansion will limit the overall durability of GSP as a roadbed filler. This is because, in practical engineering applications, GSP as a roadbed filler will encounter scenarios such as heavy rain erosion and alternation of wetting and drying, etc. Through the aforementioned research on mechanical properties, we know that, when GSP has a higher water absorption and expansion capacity, its mechanical properties are lower, without experiencing environmental changes. We believe that the low mechanical properties of GSP are due to the decrease in its overall porosity. When experiencing changes in the external environment, such as water erosion, a higher water absorption and expansion will gradually increase the porosity of GSP. This process is not recoverable. That is to say, high porosity will make GSP less resistant to water erosion, and water erosion will gradually increase the porosity of GSP. This is a mutually reinforcing process. A completed road usually needs to be used for more than a year, which means that over time the potential frequency of experiencing heavy rain erosion increases. This will break up its long-term performance.

3.2.2. The Properties of GSP after Soaking in Water

(1) Softening coefficient

It is clear from Figure 7 that, as the PG content rises, the GSP′s softening coefficient falls. The softening coefficient of GSP with 90% PG content is high, and after soaking in water for 7 d, the softening coefficient of P90-G (30:70)-C11 is 80.5%. The softening coefficient of GSP samples with 94% and 98% PG content reduced dramatically when compared to that of GSP samples with 90% PG content, particularly for the group with a higher FA amount, where the softening coefficient of P98-G(55:45)-C11 decreased by about 40% when compared to P90-G(55:45)-C11. When the PG content is increased, the softening coefficient of GSP in group G(30:70)-C11 decreases, but it usually remains steady, outperforming other groups. Oddly, the softening coefficient of GSP did not increase with the addition of a little alkalin-activator. Each group of GSP samples′ softening coefficient also steadily decreases with soaking time, and the GSP softening coefficient rapidly declines between 7 and 14 d. After 14 d, the rate of softening coefficient decrease slows, and after 60 d the softening coefficient tends to stabilize. It is clear that the soaking has a considerable effect on the UCS of GSP samples between the ages of 7 and 14 d, but that effect is much less obvious after that period. This might be because GSPs lose strength quickly when in contact with water in the early stages, but the speed of strength loss does not increase with soaking time, which is sufficient to demonstrate their capacity to maintain their mechanical properties even after prolonged soaking. At each soaking period of the experiment, no looseness was discovered in the GSP samples.

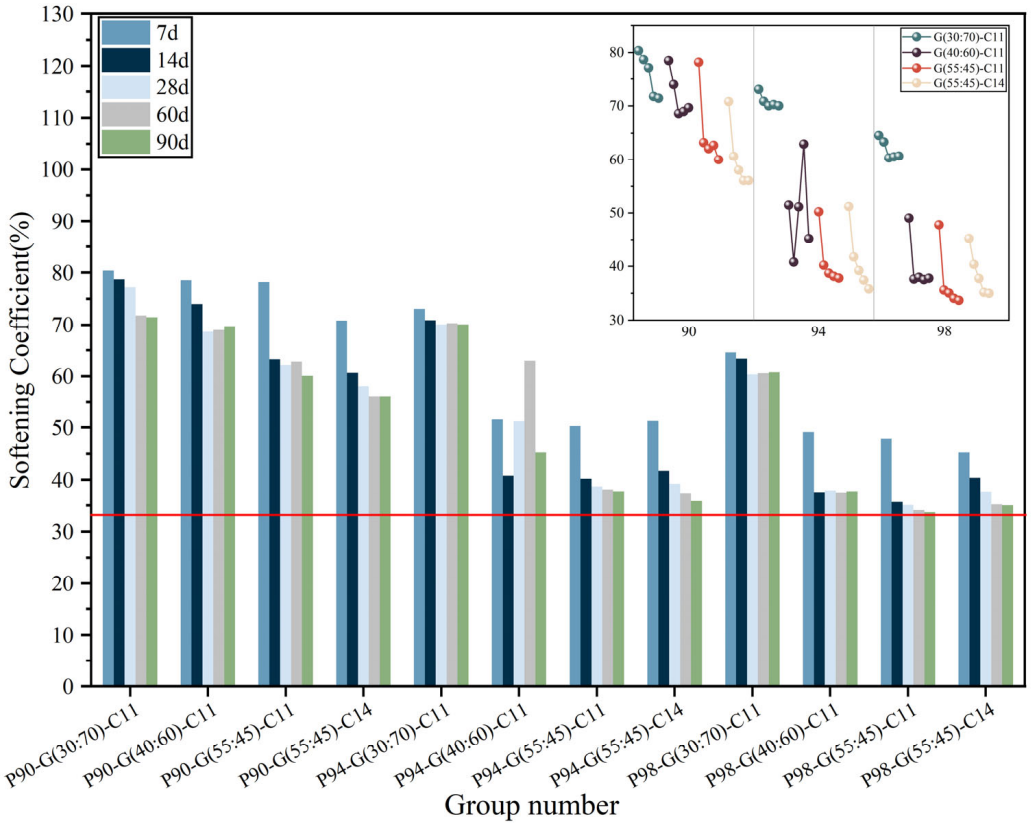

Figure 7. Softening coefficient of GSP.

(2) Mass loss rate after soaking in water (*MLRs*)

The *MLRs* of GSP samples at different soaking ages are shown in Figure 8. Figure 8a shows that, after three days of soaking in water, the *MLR* of GSP samples is negative. This is due to the fact that the mass increase phenomenon brought on by water absorption occur. When the GSP samples are soaked in water, the *MLRs* at 3 d are less than −10%, showing that the GSP samples contain numerous pores that allow it to absorb a lot of water when it first comes into contact. The P90-G(30:70)-C11 has the smallest absolute value of *MLRs* in 3 d, indicating a higher compactness. The *MLRs* of GSP samples from 6 d to 90 d fluctuate between 0.5% and 7%, but almost always stays near 0.5%. After soaking in water for a certain time, it is known that the mass loss of GSP samples will remain stable, indicating that the GSP samples still have high integrity and will not loosen or peel off in significant amounts. Figure 8b–d shows that the G(30:70)-C11 group, which exhibit superior mechanical properties, has fewer *MLRs* than other groups. Moreover, compared to other groups, the *MLRs* of the G(30:70)-C11 group are more stable as the PG content increases.

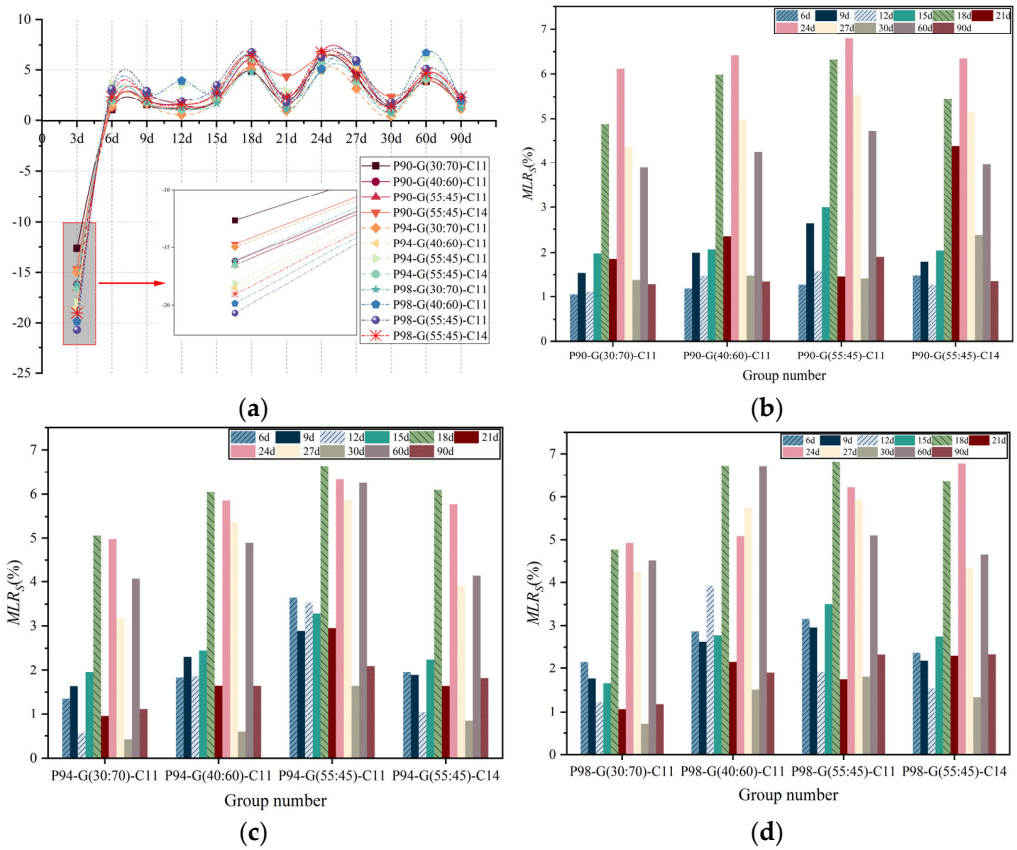

Figure 8. *MLRs* of GSP. (**a**) GSP with different ratios of PG; (**b**) GSP with 90 wt% PG; (**c**) GSP with 94 wt% PG; (**d**) GSP with 98 wt% PG.

3.2.3. Dry and Wet Cycles (DWC)

The MLR_{DWC} of GSP samples steadily declines with the *DWC*, as seen in Figures 9a and 10a, whereas the SLR_{DWC} gradually rises. When the number of cycles is between 5 and 15, the MLR_{DWC} decreases more quickly, while the SLR_{DWC} grows faster; after 15 cycles, the MLR_{DWC} and SLR_{DWC} curves tend to flatten out, and the rate of change significantly decreases. While SLR_{DWC} stayed essentially stable and even indicated a reduction after 25 cycles, MLR_{DWC} essentially remained unchanged and stabilized within 2%. The MLR_{DWC} of different groups of GSP samples increasingly approaches zero as the number of cycles rises, and the SLR_{DWC} gradually stabilizes at a particular value.

Figures 9b–d and 10b–d show that, for a constant PG content, the MLR_{DWC} and SLR_{DWC} of GSP samples increase as the FA content in the geopolymer increases. After five *DWC*, the MLR_{DWC} and SLR_{DWC} of group G(30:70)-C11 were the lowest, at 4.3% and 9.8%, respectively. The MLR_{DWC} and SLR_{DWC} of the other three groups significantly increased with the increase in PG contents, in addition to the G(30:70)-C11 groups. For instance, the G(30:70)-C11 group grew by 8% with the rise in the mass percentage of PG, but its mass loss rate only increased by 18.6%. In contrast, the MLR_{DWC} of P98-G(55:45)-C11 increased by 67.8% compared with P90-G(55:45)-C11. The MLR_{DWC} and SLR_{DWC} of GSP samples are also decreased by the addition of a slight amount of alkali-activator. Figures 9a and 10a show the stability of GSP samples under *DWC*, with the G(30:70)-C11 group showing the best stability. The *MLR* of GSP in soaking or *DWC* tests is less than 7%, and this material is considered durable according to ASTM D559/D559 M [48].

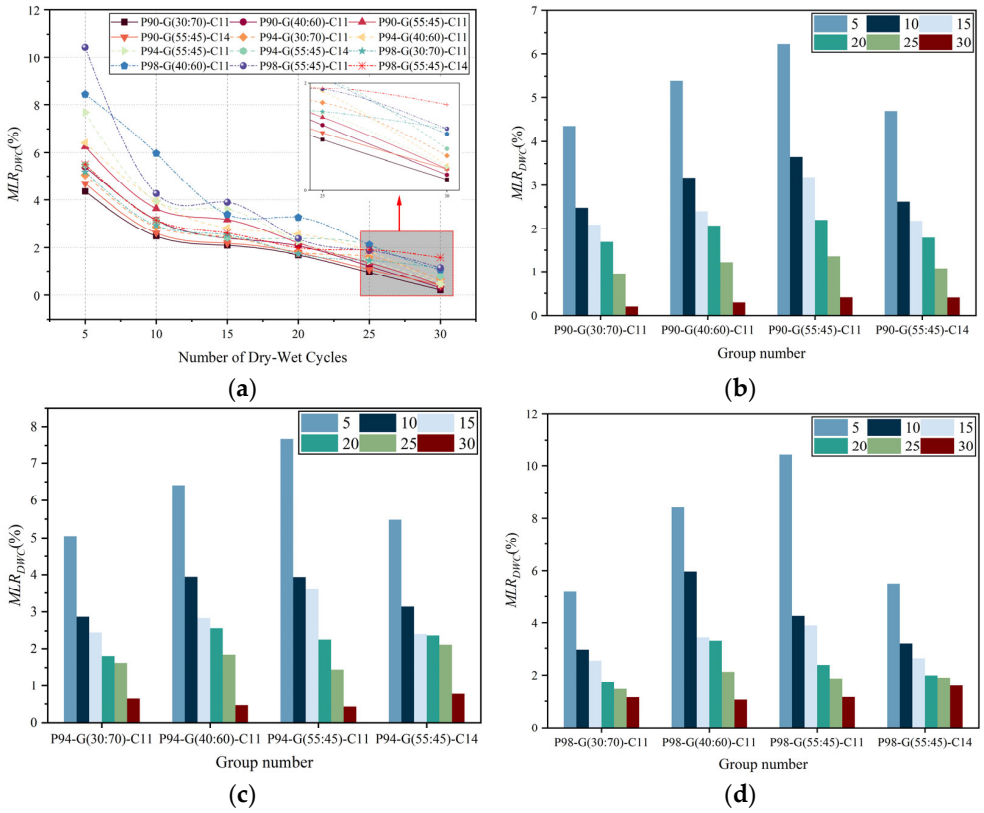

Figure 9. MLR_{DWC} of GSP after *DWC*. (**a**) GSP with different ratios of PG; (**b**) GSP with 90wt% PG; (**c**) GSP with 94wt% PG; (**d**) GSP with 98wt% PG.

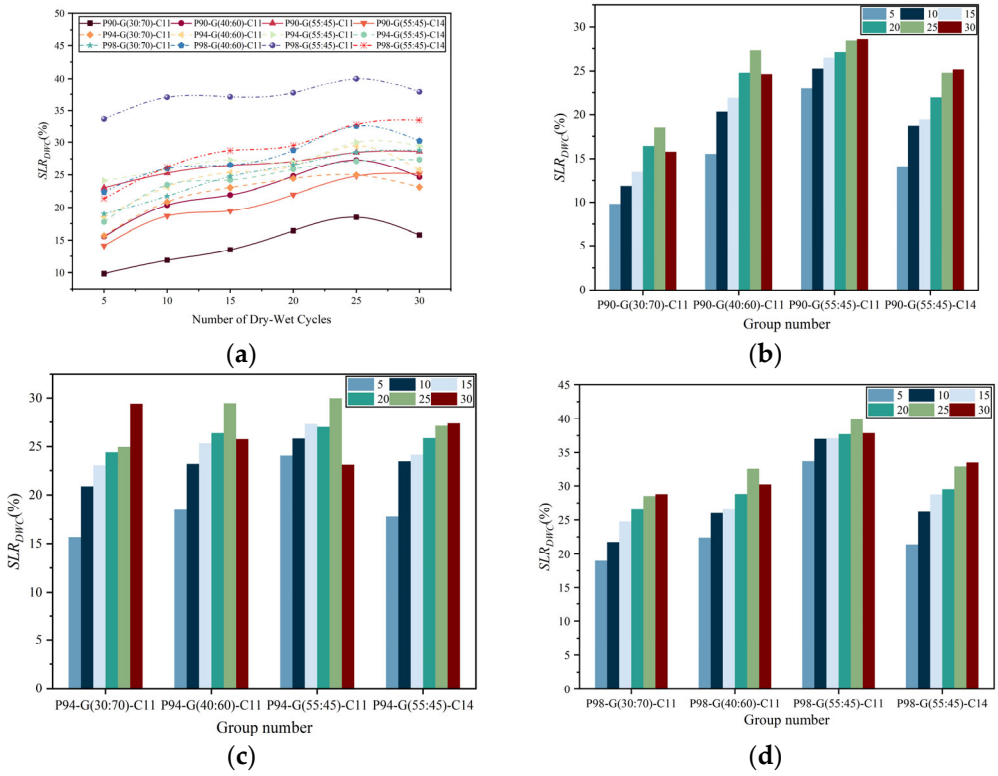

Figure 10. SLR_{DWC} of GSP after *DWC*. (**a**) GSP with different ratios of PG; (**b**) GSP with 90wt% PG; (**c**) GSP with 94wt% PG; (**d**) GSP with 98wt% PG.

3.2.4. Discussion

The *MLR* and *SLR* of the GSP during soaking or *DWC* is primarily affected by the porosity of GSP. Through the discussion in Section 3.1.4, we believe that the better the mechanical properties of GSP, the lower its porosity. By combining the results for water stability with the mechanical properties, a positive correlation can be observed between the two. PG solubility is also influenced by the pH and soluble phosphorus [47]. For this reason, the GSP group with better mechanical properties also has a lower *MLR*. The higher the PG content, the higher the content of unreacted PG in the GSP. A higher concentration of soluble phosphorus and a lower pH value in GSP as a result of the rise in unreacted PG will lead to decreased solubility of PG. As a result, a greater amount of PG will dissolve, and the *MLR* and *SLR* will rise. The compactness of GSP decreases, the number of pores rises, and the size of the pores expands. The result is an increase in the *MLR* and *SLR* of GSP and a greater surface area of water molecules in contact with unreacted PG. Furthermore, the volume stability and strength stability of GSP become worse.

Secondly, the most obvious consequence of adding more alkali-activator is an increase in the overall pH of hydration environment, which makes PG comparatively less soluble [45]. At the same time, the increase in pH value will promote the hydration reaction, resulting in more hydration products with cementitious properties in GSP. The increase in pH value will promote the hydration reaction, resulting in more hydration products with cementitious properties in GSP.

Additionally, the mass loss of GSP will increase the number of pores in GSP, resulting in a fall in the softening coefficient and strength loss rate during *DWC* or soaking. This is because the water stability and durability of GSP simulate its ability to maintain its own mechanical properties when facing environmental changes in road construction and maintenance.

3.3. Discussion of Strength Formation Mechanism

3.3.1. XRD

The X-ray diffraction patterns of each group of GSP samples at 60 d are shown in Figure 11. The mineral composition of GSP samples is $CaSO_4 \cdot 2H_2O$, ettringite, C-S-H, and a little quartz. As seen in Figure 11a–c, $CaSO_4 \cdot 2H_2O$ are followed by ettringite, which has numerous and relatively high peaks. This reveals that $CaSO_4 \cdot 2H_2O$, followed by ettringite is the most abundant mineral component in the GSP. This is mainly because the GSP sample contains more PG as fine aggregate, and the primary component of PG is $CaSO_4 \cdot 2H_2O$. The formation of ettringite resulted from a dissolution-polycondensation that occurred as the mechanical properties of GSP were being developed. C-A-H, C-S-H, C-A-S-H, and N-A-S-H are the four polymers that should be present in the hydration products, according to Section 3.1.4. Furthermore, C-A-H can be hydrated with the sulfate in PG to form the precipitation of ettringite [49–51].

In Figure 11d, we conducted a semi-quantitative analysis of the XRD results of GSP samples. Figure 11d illustrates that, when the content of ettringite in GSP samples increases, the content of $CaSO_4 \cdot 2H_2O$ decreases. The two show opposite trends. This is because, during the hydration reaction of GSP, the formation of ettringite requires the consumption of calcium ions and sulfate ions provided by gypsum. Moreover, Figure 11 shows that the relative content of ettringite is proportional to the mechanical properties and water stability of GSP, which is adequate to explain the reliability of Sections 3.1.4 and 3.2.4. The content of ettringite will increase when the proportion of GBFS in GSP increases, or the proportion of PG decreases, or the amount of alkali-activator appropriately rises, improving the mechanical properties and water stability of GSP.

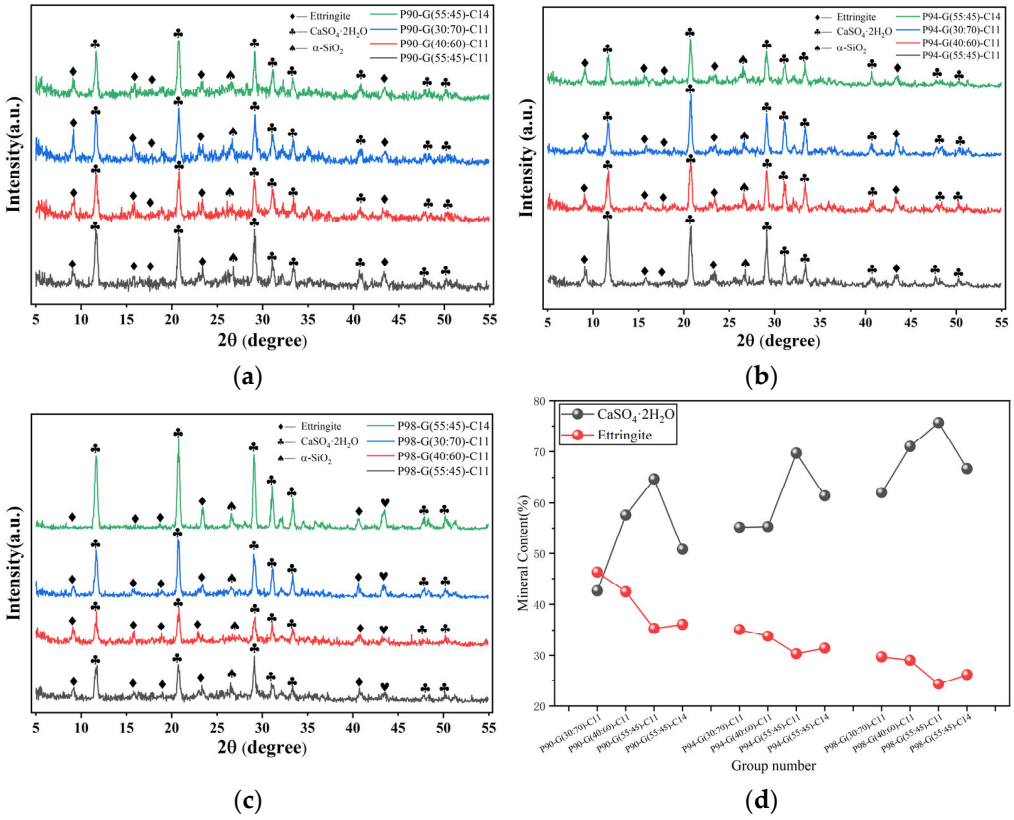

Figure 11. XRD (**a**–**c**) and mineral content (**d**) of GSP.

3.3.2. SEM

Figure 12 depicts the microstructure of P94-G(30:70)-C11 at different ages. At the age of 3 d, lamellar or columnar gypsum crystals are joined together under compaction, as seen in Figure 12a,b, the gel structure is tidy and there is a lot of FA microsphere present. A honeycomb-like gel material with a complete structure but a small amount was generated at the age of 7 d, and a small amount of needle-like ettringite was attached to the surface of the gypsum crystal. A significant amount of honeycomb-like gel was formed at the age of 14 d, no FA particles were seen, and a significant amount of needle-like ettringite was generated and covered in gypsum crystals. At 28 d, the honeycomb-like gel began to accumulate into flocculent material. This flocculent material adhered to the surface of gypsum crystals, connecting them into aggregates, which then continued to bind the crystals together to form larger particles. A portion of the gypsum crystals participates in the hydration reaction to form needle-like ettringite crystals and C-S-H gel. In the remaining residual gypsum crystals in GSP, some are bound by the flocculent gel to form aggregates, some fill the pores of the structure as shown in Figure 12i, and some are covered by needle-like ettringite and interspersed within its pores to form a dense structure, as shown in Figure 12j.

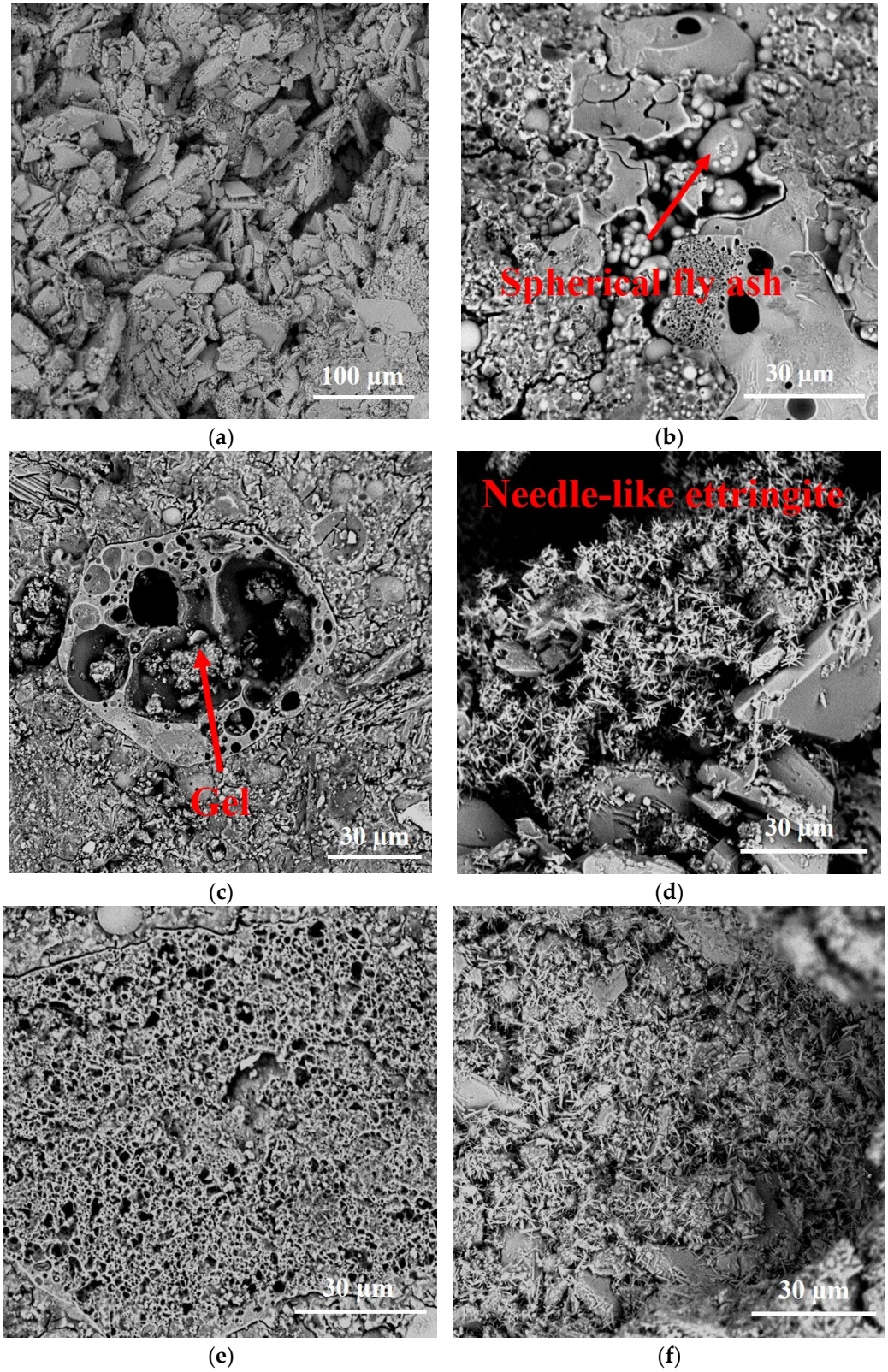

Figure 12. *Cont.*

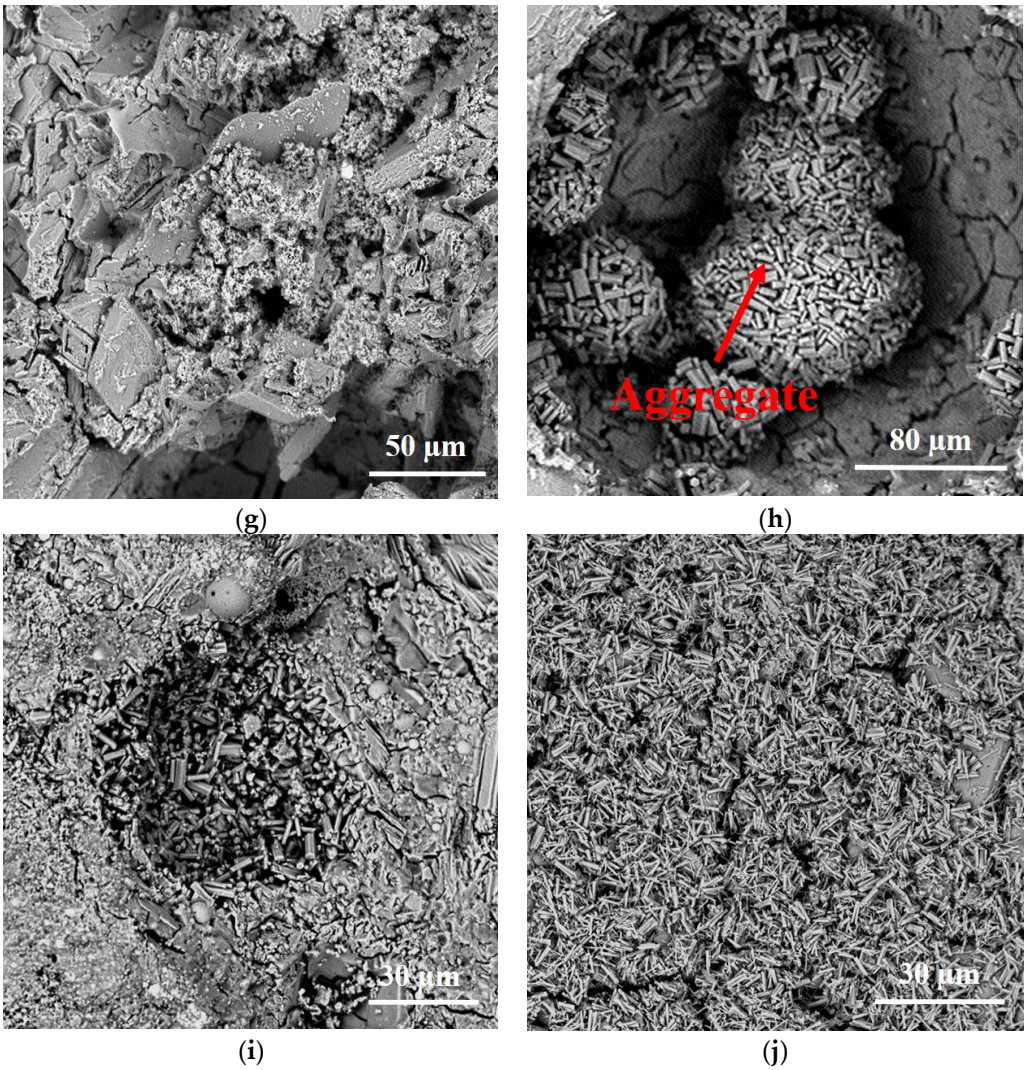

Figure 12. SEM of GSP. (**a**) P94-G(30:70)-C11-3d; (**b**) P94-G(30:70)-C11-3d; (**c**) P94-G(30:70)-C11-7d; (**d**) P94-G(30:70)-C11-7d; (**e**) P94-G(30:70)-C11-14d; (**f**) P94-G(30:70)-C11-14d; (**g**) P94-G(30:70)-C11-28d; (**h**) P94-G(30:70)-C11-28d; (**i**) P94-G(30:70)-C11-60d; (**j**) P94-G(30:70)-C11-60d.

3.3.3. Strength Formation Mechanism

It can be concluded that the way that geopolymers stabilize PG is not only through a single action, but also through the combination of chemical reaction and physical action based on the result:

(1) Physical action: the physical properties of the GSP, such as particle size distribution, plasticity, and compaction throughout the molding process, are a reflection of the physical action [47,52].

(2) Chemical reaction: GSP uses geopolymer as a curing agent to solidify PG as a roadbed filler. It takes into account the hydration products formed by geopolymer, which can react with PG to create a further hydration reaction to form ettringite and support the development of strength, in addition to the chemical cementation action of geopolymer. PG serves as a sulfate activator and a calcium source in this process, and water glass and sodium hydroxide serve as alkali-activator in this study. A few sources of silicon can also be found in a water glass at the same time. Lastly, with GBFS and FA, two potentially active alumino-silicate materials, ion dissolution and ion exchange will take place to generate C-S-H gel, N-A-S-H gel and ettringite under the double activation of sulfate and alkaline [17].

(3) A combination of chemical reactions and physical actions: we believe that physical actions and chemical reactions in GSP promote strength development by, together, decreasing the porosity in GSP. Ettringite can fill the pores between PG particles thanks to its minor expansibility, and C-S-H gel with cementation property can connect dispersed PG particles, which promotes the development of strength [53]. The fewer number of pores and smaller pore size of the solidified soil when an equal amount of hydration products are produced, the larger the increase in density of the hydration products that fill the pores between particles and, hence, the more powerful the cementation effect the hydration products produce. This may encourage the initially distributed PG particles to cluster tightly together [54]. The large development and excessive expansion of ettringite in low-porosity soils, however, might cause disruption and splitting of solidified soil in the late stages of curing, which can cause strength reversion [55].

Firstly, it is clear from the SEM of GSP (Figure 12) that the GSP's physical mechanical properties gradually become completely developed. This strength growth is mostly attributable to the initial cation exchange and flocculation inside the GSP matrix, as well as the cementation between non-reacting particles and the gelling compound during the curing process [56]. From the observation of the micromorphology of GSP, the presence of cementation products was found. The primary and secondary cementation products generated by hydration reactions are primarily responsible for the early and long-term strength development of GSP [57]. The size and number of pores in GSP are nearly constant under identical physical conditions, and hence the yield of cementation products (i.e., CSH, CAH, and Aft) has the biggest impact on the strength development.

The Ca-Na-Si-Al quaternary system, which is primarily made of geopolymers and partially supplied with calcium by PG, produces the majority of the primary cementation products. In a system dominated by geopolymers, a reaction called dissolution-polycondensation takes place [58]. Thanks to the sulfate provided by the PG and the alkaline environment provided by the alkali-activator, the GBFS has undergone dissolution during this process, which also stimulates the potential activity of the FA and encourages the occurrence of polycondensation reactions [17]. The following are the reaction Equations (7)–(12) [39,59]. The gels C-A-H, C-S-H, C-A-S-H, and N-A-S-H are formed during this process. The system is capable of producing the four gels. These four gels live side by side and interact with one another. Together, these cementitious materials aggregate loose PG particles, cover PG particles' surfaces, and fill in GSP's pores, strengthening the link between the two materials and promoting GSP's potential to become denser [60]. The GSP's residual unreacted FA and GBFS particles fill the space, which also lowers the soil's porosity and enhances the strength of the GSP.

Calcium, aluminum, and silicon sources in the GSP system dissolve:

$$SiO_2 + Al_2O_3 \xrightarrow{OH^-} SiO_2(OH)_2{}^{2-} \text{or } SiO(OH)_3{}^- + Al(OH)_4^- \quad (7)$$

$$CaSO_4, CaO \xrightarrow{H_2O} Ca^{2+} + SO_4{}^{2-} + OH^- \quad (8)$$

Predicted hydration reaction:

$$Ca^{2+} + SiO_2(OH)_2{}^{2-} \text{or } SiO(OH)_3{}^- + Al(OH)_4{}^- \longrightarrow \text{CASHgel} \quad (9)$$

$$Na^+ + SiO_2(OH)_2{}^{2-} \text{or } SiO(OH)_3{}^- + Al(OH)_4{}^- \longrightarrow \text{NASHgel} \quad (10)$$

$$3Ca(OH)_2 + SiO_2 + (n-3)H_2O \longrightarrow 3CaSiO_2 \cdot nH_2O \quad (11)$$

$$3Ca(OH)_2 + Al_2O_3 + (n-3)H_2O \longrightarrow 3CaAl_2O_3 \cdot nH_2O \quad (12)$$

From the XRD analysis of GSP (Figure 11), we observed more secondary cementation products (ettringite), produced by the hydration reaction between the sulfate provided by PG in the GSP and the primary cementation product generated by the geopolymer, as indicated in Equation (13). Early strength development is significantly benefited by ettringite. It is a calcium aluminum sulfate mineral that has adhesion and micro-expansion characteristics [52]. In between the pores of the GSP and other cementation products, the ettringite crystal undergoes a micro-expansion effect that promotes strength development through processes including cementation, overlapping, interlocking, and pore filling [61].

$$3CaO \cdot Al_2O_3 \cdot nH_2O + 3CaSO_4 \cdot 2H_2O + (26 - n)H_2O \rightarrow 3CaO \cdot Al_2O_3 \cdot 3CaSO_4 \cdot 32H_2O \quad (13)$$

Overall, physical compaction, chemical excitation, ion exchange, bonding between the gel and the ettringite, agglomeration, and physical filling are the primary processes involved in the development of the mechanical properties of GSP. The mechanical properties of GSP directly correlate with its water stability and durability. From a microscopic standpoint, Figure 13 depicts the process of GSP strength development.

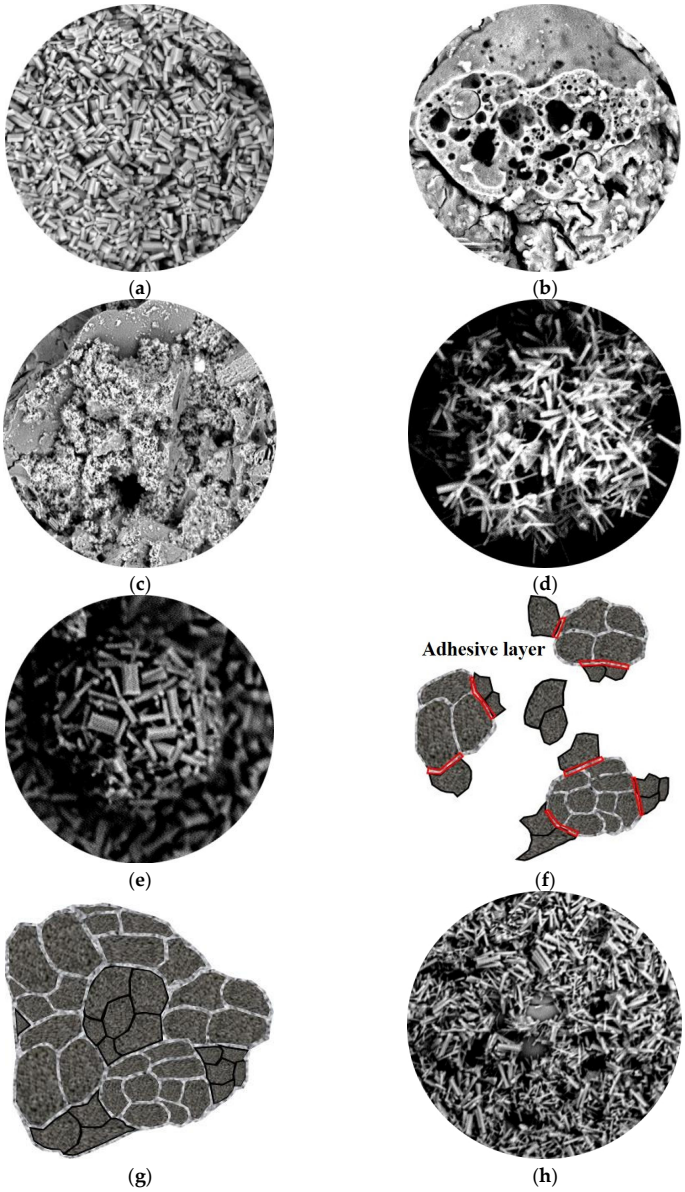

Figure 13. *Cont.*

(**i**)

Figure 13. Strength formation mechanism of the GSP. (**a**) Physical compaction; (**b**) Honeycomb-like gel; (**c**) Flocculent gel linked to gypsum crystals; (**d**) Ettringite bonded gypsum crystals; (**e**) Aggregation; (**f**) Aggregation bonded gypsum crystals; (**g**) Aggregation embedding; (**h**) Ettringite-filled pores; (**i**) Gypsum-filled pores.

Physical compaction: after the GSP was compacted and formed, as shown in Figure 13a, gypsum particles were closely embedded with one another inside the stabilized body, although some of the gypsum particles had voids between them.

Ion exchange and chemical activation: as depicted in Figure 13b, in an alkaline environment, the active ingredients SiO_2, Al_2O_3, and CaO in the raw material are activated by the alkali-activator to produce a honeycomb-like network gel with colloidal properties and needle-like ettringite crystals through ion exchange.

Gel and ettringite bonding: as shown in Figure 13c,d, under the action of cementation, the honeycomb-like three-dimensional mesh gel is connected and polymerized to create a large number of flocculent gel polymers. These polymers adhere to the surface of gypsum, and the needle-like ettringite is also adherent to the surface of gypsum.

Aggregation: as depicted in Figure 13e–g, numerous gel aggregates gradually wrap and cover the gypsum particles by adhering to their surface. The gel-wrapped gypsum particles are covered by gel bonding into a new gel-bonded layer, which can still connect the gypsum particles. Through this cycle, the aggregates with particle gradation are formed by adhering in turn, and these particles of different sizes are embedded with each other to form a spatial skeleton structure.

Physical filling: as shown in Figure 13h,i, a large number of remaining gypsum particles are embedded in each other and filled in the pores of the aggregate skeleton, while fine needle-like ettringite crystals fill the pores of GSP, forming a dense skeletal space structure.

The mechanism of the geopolymer stabilizing PG is predominantly through forming more aggregates by gels and ettringite cover gypsum particles, by filling the pores in GSP to improve its denseness. PG in the stabilized material not only plays a skeleton role but also carries on a hydration reaction with geopolymer to form the ettringite filling skeleton.

4. Conclusions

The following are the main conclusions of this study:

(1) The content of geopolymer, the ratio of FA to GBFS in geopolymer, and the amount of alkali-activator in geopolymer all affect the mechanical properties of GSP. When the content of geopolymer increases, or the ratio of FA to GBFS decreases, or the alkali-activator increases, the mechanical properties of GSP will be better developed.

(2) Physical compaction, chemical activation and ion exchange, gel and ettringite bonding, aggregation, and physical filling to produce a dense structure are the primary processes involved in the development of the mechanical strength of GSP.

(3) There is a positive correlation between the mechanical properties, water stability, and durability of GSP. This is because all three properties are affected by the overall compactness of GSP. When the porosity in GSP is lower, its mechanical properties

develop better and are less affected by the external environment, thus maintaining long-term mechanical properties.

(4) The lower the ratio of FA to GBFS in geopolymer, the better the curing effect of GSP. This is because more FA results in less calcium and the FA utilized in this study has a low calcium content. N-A-S-H is now primarily produced to provide the geopolymer strength, but it does not act to bind the PG particles or allow for additional chemical reactions with the PG in the GSP.

(5) The proper increase of alkali-activator mainly affects the stability effect of GSP by adjusting the pH of the overall hydration environment of GSP. The increase of pH will promote the rapid dissolution of ions in raw materials and further promote their ion exchange to form ettringite or C-S-H gel.

(6) The possibility of GSP being implemented in practical engineering projects. This is because the pre-treatment process of GSP only requires sieving treatment of PG and adjusting the ratio in the geopolymer as a curing agent.

Author Contributions: Methodology, data curation, formal analysis, writing—original draft, Writing—review and editing, writing—original draft, Y.W.; formal analysis, H.Z.; Writing—review and editing, H.L. (Haikun Lin); data curation, X.W.; Methodology, H.L. (Heng Li); validation, Y.L.; data curation, J.X. and S.C.; data curation, G.G.; investigation, H.T., H.H. and W.Z.; supervision, funding acquisition, F.X. All authors have read and agreed to the published version of the manuscript.

Funding: This work was supported by Science and Technology Project of Wuyang Expressway, Science and Technology Project of Hubei Transportation Department (2022-11-6-1), Enterprise Technology Innovation Project of Shandong Province (202160101791) and the Science and Technology Project of Shandong Expressway Bridge Maintenance Co., Ltd. (2021-06).

Institutional Review Board Statement: Not applicable.

Informed Consent Statement: Not applicable.

Data Availability Statement: The data presented in this study are available on request from the corresponding author.

Conflicts of Interest: The authors declare no conflict of interest.

References

1. Ferreira, D.F.S.; Oliveira, W.D.; Siqueira, M.R.S.; Silva, C.A.B.; Del Nero, J. Electronic confinement in α-pho-graphene devices by hydrogenation and width effect consonance. *Mater. Lett.* **2023**, *347*, 134609. [CrossRef]
2. Contreras, M.; Pérez-López, R.; Gázquez, M.J.; Morales-Flórez, V.; Santos, A.; Esquivias, L.; Bolívar, J.P. Fractionation and fluxes of metals and radionuclides during the recycling process of phosphogypsum wastes applied to mineral CO_2 sequestration. *Waste Manag.* **2015**, *45*, 412–419. [CrossRef] [PubMed]
3. Shen, W.; Gan, G.; Dong, R.; Chen, H.; Tan, Y.; Zhou, M. Utilization of solidified phosphogypsum as Portland cement retarder. *J. Mater. Cycles Waste Manag.* **2012**, *14*, 228–233. [CrossRef]
4. Mehta, P.K.; Brady, J.R. Utilization of phosphogypsum in portland cement industry. *Cem. Concr. Res.* **1977**, *7*, 537–544. [CrossRef]
5. Ölmez, H.; Erdem, E. The effects of phosphogypsum on the setting and mechanical properties of Portland cement and trass cement. *Cem. Concr. Res.* **1989**, *19*, 377–384. [CrossRef]
6. Ölmez, H.; Yilmaz, V.T. Infrared study on the refinement of phosphogypsum for cements. *Cem. Concr. Res.* **1988**, *18*, 449–454. [CrossRef]
7. Zeng, L.-L.; Bian, X.; Zhao, L.; Wang, Y.-J.; Hong, Z.-S. Effect of phosphogypsum on physiochemical and mechanical behaviour of cement stabilized dredged soil from Fuzhou, China. *Geomech. Energy Environ.* **2021**, *25*, 100195. [CrossRef]
8. Rashad, A.M. Phosphogypsum as a construction material. *J. Clean. Prod.* **2017**, *166*, 732–743. [CrossRef]
9. Tayibi, H.; Choura, M.; López, F.A.; Alguacil, F.J.; López-Delgado, A. Environmental impact and management of phosphogypsum. *J. Environ. Manag.* **2009**, *90*, 2377–2386. [CrossRef]
10. Papaslioti, E.-M.; Pérez-López, R.; Parviainen, A.; Sarmiento, A.M.; Nieto, J.M.; Marchesi, C.; Delgado-Huertas, A.; Garrido, C.J. Effects of seawater mixing on the mobility of trace elements in acid phosphogypsum leachates. *Mar. Pollut. Bull.* **2018**, *127*, 695–703. [CrossRef]
11. Lütke, S.F.; Oliveira, M.L.S.; Silva, L.F.O.; Cadaval, T.R.S.; Dotto, G.L. Nanominerals assemblages and hazardous elements assessment in phosphogypsum from an abandoned phosphate fertilizer industry. *Chemosphere* **2020**, *256*, 127138. [CrossRef] [PubMed]

12. Jalali, J.; Gaudin, P.; Capiaux, H.; Ammar, E.; Lebeau, T. Fate and transport of metal trace elements from phosphogypsum piles in Tunisia and their impact on soil bacteria and wild plants. *Ecotoxicol. Environ. Saf.* **2019**, *174*, 12–25. [CrossRef] [PubMed]
13. Ngo, H.T.T.; Dang, V.Q.; Ho, L.S.; Doan, T.X. Utilization phosphogypsum as a construction material for road base: A case study in Vietnam. *Innov. Infrastruct. Solut.* **2021**, *7*, 88. [CrossRef]
14. Meskini, S.; Samdi, A.; Ejjaouani, H.; Remmal, T. Valorization of phosphogypsum as a road material: Stabilizing effect of fly ash and lime additives on strength and durability. *J. Clean. Prod.* **2021**, *323*, 129161. [CrossRef]
15. Calderón-Morales, B.R.S.; García-Martínez, A.; Pineda, P.; García-Tenório, R. Valorization of phosphogypsum in cement-based materials: Limits and potential in eco-efficient construction. *J. Build. Eng.* **2021**, *44*, 102506. [CrossRef]
16. Gu, Z.; Fang, A.; Hua, S.; Zhao, Q.; Sun, L.; Xia, F.; Qian, L.; Ren, X. Development of a Soil Stabilizer for Road Subgrade Based on Original Phosphogypsum. *J. Renew. Mater.* **2021**, *9*, 253–268. [CrossRef]
17. Mun, K.J.; Hyoung, W.K.; Lee, C.W.; So, S.Y.; Soh, Y.S. Basic properties of non-sintering cement using phosphogypsum and waste lime as activator. *Constr. Build. Mater.* **2007**, *21*, 1342–1350. [CrossRef]
18. Shen, W.; Zhou, M.; Zhao, Q. Study on lime–fly ash–phosphogypsum binder. *Constr. Build. Mater.* **2007**, *21*, 1480–1485. [CrossRef]
19. Shen, W.; Zhou, M.; Ma, W.; Hu, J.; Cai, Z. Investigation on the application of steel slag–fly ash–phosphogypsum solidified material as road base material. *J. Hazard. Mater.* **2009**, *164*, 99–104. [CrossRef]
20. Parreira, A.B.; Kobayashi, A.R.K.; Silvestre, O.B. Influence of Portland Cement Type on Unconfined Compressive Strength and Linear Expansion of Cement-Stabilized Phosphogypsum. *J. Environ. Eng.* **2003**, *129*, 956–960. [CrossRef]
21. Liu, Y.; Zhang, D.; You, L.; Luo, H.; Xu, W. Recycling phosphogypsum in subbase of pavement: Treatment, testing, and application. *Constr. Build. Mater.* **2022**, *342*, 127948. [CrossRef]
22. Wang, Y.; Wang, X.; Ning, M.; He, J.; He, J.; Lei, Y.; Hou, S. The collaborative pollutants and carbon dioxide emission reduction and cost of ultra-low pollutant emission retrofit in China's cement kiln. *J. Clean. Prod.* **2023**, *405*, 136939. [CrossRef]
23. Davidovits, J.; Huaman, L.; Davidovits, R. Ancient organo-mineral geopolymer in South-American Monuments: Organic matter in andesite stone. SEM and petrographic evidence. *Ceram. Int.* **2019**, *45*, 7385–7389. [CrossRef]
24. Silva, P.D.; Sagoe-Crenstil, K.; Sirivivatnanon, V. Kinetics of geopolymerization: Role of Al_2O_3 and SiO_2. *Cem. Concr. Res.* **2007**, *37*, 512–518. [CrossRef]
25. Gu, G.; Pei, Y.; Ma, T.; Chen, F.; Zhang, J.; Xu, F. Role of carbon fiber in the electrothermal behavior and geopolymerization process of carbon fiber-reinforced FA-GBFS geopolymer composite. *Constr. Build. Mater.* **2023**, *369*, 130597. [CrossRef]
26. Gu, G.; Ma, T.; Chen, F.; Li, H.; Pei, Y.; Xu, F. Soft magnetic geopolymer in airport pavement induction heating: Effect of Fe powder distribution on the electromagnetic loss. *Ceram. Int.* **2023**, *49*, 1720–1730. [CrossRef]
27. Gu, G.; Ma, T.; Chen, F.; Xu, F.; Zhang, J. Electromagnetic and mechanical properties of FA-GBFS geopolymer composite used for induction heating of airport pavement. *Cem. Concr. Compos.* **2022**, *129*, 104503. [CrossRef]
28. *GB/T 23456-2018*; Phosphogypsum. Standard in China: Beijing, China, 2018.
29. Xu, F.; Li, H.; Sun, T.; Zhou, Y.; Zhu, J.; Peng, C.; Lin, J. Enhancing the mechanical and durability properties of fly ash-based geopolymer mortar modified by polyvinyl alcohol fibers and styrene butadiene rubber latex. *Mater. Express* **2021**, *11*, 1453–1465. [CrossRef]
30. Li, H.; Gao, P.; Xu, F.; Sun, T.; Zhou, Y.; Zhu, J.; Peng, C.; Lin, J. Effect of Fine Aggregate Particle Characteristics on Mechanical Properties of Fly Ash-Based Geopolymer Mortar. *Minerals* **2021**, *11*, 897. [CrossRef]
31. Xu, F.; Deng, X.; Peng, C.; Zhu, J.; Chen, J. Mix design and flexural toughness of PVA fiber reinforced fly ash-geopolymer composites. *Constr. Build. Mater.* **2017**, *150*, 179–189. [CrossRef]
32. Gu, G.; Xu, F.; Ruan, S.; Huang, X.; Zhu, J.; Peng, C. Influence of precast foam on the pore structure and properties of fly ash-based geopolymer foams. *Constr. Build. Mater.* **2020**, *256*, 119410. [CrossRef]
33. Gu, G.; Xu, F.; Huang, X.; Ruan, S.; Peng, C.; Lin, J. Foamed geopolymer: The relationship between rheological properties of geopolymer paste and pore-formation mechanism. *J. Clean. Prod.* **2020**, *277*, 123238. [CrossRef]
34. *JTG 3430-2020*; Test Methods of Soils for Highway Engineering. Standard in China: Beijing, China, 2020.
35. *JTG-E51-2009*; Test Methods of Materials Stabilized with Inorganic Binders for Highway Engineering. Standard in China: Beijing, China, 2009.
36. Lu, C.; Chen, J.; Gu, C.; Wang, J.; Cai, Y.; Zhang, T.; Lin, G. Resilient and permanent deformation behaviors of construction and demolition wastes in unbound pavement base and subbase applications. *Transp. Geotech.* **2021**, *28*, 100541. [CrossRef]
37. *JTG/T 3610-2019*; Technical Specifications for Construction of Highway Subgrades. Standard in China: Beijing, China, 2019.
38. Sivapullaiah, P.V.; Sridharan, A.; Raju, K.V.B. Role of amount and type of clay in the lime stabilization of soils. *Proc. Inst. Civil. Eng. Ground Improv.* **2000**, *4*, 37–45. [CrossRef]
39. Gao, X.; Yu, Q.L.; Brouwers, H.J.H. Reaction kinetics, gel character and strength of ambient temperature cured alkali activated slag–fly ash blends. *Constr. Build. Mater.* **2015**, *80*, 105–115. [CrossRef]
40. Granizo, M.L.; Alonso, S.; Blanco-Varela, M.T.; Palomo, A. Alkaline Activation of Metakaolin: Effect of Calcium Hydroxide in the Products of Reaction. *J. Am. Ceram. Soc.* **2002**, *85*, 225–231. [CrossRef]
41. Alexander, A.E.; Shashikala, A.P. Studies on the microstructure and durability characteristics of ambient cured FA-GGBS based geopolymer mortar. *Constr. Build. Mater.* **2022**, *347*, 128538. [CrossRef]
42. Görhan, G.; Kürklü, G. The influence of the NaOH solution on the properties of the fly ash-based geopolymer mortar cured at different temperatures. *Compos. Part. B Eng.* **2014**, *58*, 371–377. [CrossRef]

43. Fernández-Jiménez, A.; Palomo, A. Composition and microstructure of alkali activated fly ash binder: Effect of the activator. *Cem. Concr. Res.* **2005**, *35*, 1984–1992. [CrossRef]
44. Phair, J.W.; Van Deventer, J.S.J. Effect of silicate activator pH on the leaching and material characteristics of waste-based inorganic polymers. *Miner. Eng.* **2001**, *14*, 289–304. [CrossRef]
45. Shekhovtsova, J.; Kearsley, E.P.; Kovtun, M. Effect of activator dosage, water-to-binder-solids ratio, temperature and duration of elevated temperature curing on the compressive strength of alkali-activated fly ash cement pastes. *J. S. Afr. Inst. Civ. Eng.* **2014**, *56*, 44–52.
46. Heah, C.Y.; Kamarudin, H.; Bakri, A.M.M.A.; Bnhussain, M.; Luqman, M.; Nizar, I.K.; Ruzaidi, C.M.; Liew, Y.M. Kaolin-based geopolymers with various NaOH concentrations. *Int. J. Miner. Metall. Mater.* **2013**, *20*, 313–322. [CrossRef]
47. Hammas, I.; Horchani-Naifer, K.; Férid, M. Solubility study and valorization of phosphogypsum salt solution. *Int. J. Miner. Process.* **2013**, *123*, 87–93. [CrossRef]
48. *ASTM D559/D559*; Standard Test Methods for Wetting and Drying Compacted Soil-Cement Mixtures. ASTM International: West Conshohocken, PA, USA, 2015.
49. Li, X.; Xu, F.; Chen, B.; Li, B.; Chen, Z.; Zhu, J.; Peng, C.; Lin, J. Investigation on the chloride ion erosion mechanism of cement mortar in coastal areas: From experiments to molecular dynamics simulation. *Constr. Build. Mater.* **2022**, *350*, 128810. [CrossRef]
50. Singhi, B.; Laskar, A.I.; Ahmed, M.A. Mechanical Behavior and Sulfate Resistance of Alkali Activated Stabilized Clayey Soil. *Geotech. Geol. Eng.* **2017**, *35*, 1907–1920. [CrossRef]
51. Zhang, M.; Guo, H.; El-Korchi, T.; Zhang, G.; Tao, M. Experimental feasibility study of geopolymer as the next-generation soil stabilizer. *Constr. Build. Mater.* **2013**, *47*, 1468–1478. [CrossRef]
52. Bian, X.; Zeng, L.; Ji, F.; Xie, M.; Hong, Z. Plasticity role in strength behavior of cement-phosphogypsum stabilized soils. *J. Rock. Mech. Geotech. Eng.* **2022**, *14*, 1977–1988. [CrossRef]
53. Kamruzzaman, A.H.M.; Chew, S.H.; Lee, F.H. Microstructure of cement-treated Singapore marine clay. *Proc. Inst. Civil. Eng.Ground Improv.* **2006**, *10*, 113–123. [CrossRef]
54. Sivapullaiah, P.V.; Jha, A.K. Gypsum Induced Strength Behaviour of Fly Ash-Lime Stabilized Expansive Soil. *Geotech. Geol. Eng.* **2014**, *32*, 1261–1273. [CrossRef]
55. Kuryatnyk, T.; Angulski da Luz, C.; Ambroise, J.; Pera, J. Valorization of phosphogypsum as hydraulic binder. *J. Hazard. Mater.* **2008**, *160*, 681–687. [CrossRef]
56. Cherian, C.; Arnepalli, D.N. A Critical Appraisal of the Role of Clay Mineralogy in Lime Stabilization. *Int. J. Geosynth. Ground Eng.* **2015**, *1*, 8. [CrossRef]
57. Yi, Y.; Li, C.; Liu, S.; Jin, F. Magnesium sulfate attack on clays stabilised by carbide slag- and magnesia-ground granulated blast furnace slag. *Géotechnique Lett.* **2015**, *5*, 306–312. [CrossRef]
58. Fang, Y.; Kayali, O. The fate of water in fly ash-based geopolymers. *Constr. Build. Mater.* **2013**, *39*, 89–94. [CrossRef]
59. Puligilla, S.; Mondal, P. Role of slag in microstructural development and hardening of fly ash-slag geopolymer. *Cem. Concr. Res.* **2013**, *43*, 70–80. [CrossRef]
60. Yip, C.K.; Lukey, G.C.; van Deventer, J.S.J. The coexistence of geopolymeric gel and calcium silicate hydrate at the early stage of alkaline activation. *Cem. Concr. Res.* **2005**, *35*, 1688–1697. [CrossRef]
61. Jha, A.K.; Sivapullaiah, P.V. Physical and strength development in lime treated gypseous soil with fly ash—Micro-analyses. *Appl. Clay Sci.* **2017**, *145*, 17–27. [CrossRef]